The Canadian Mineralogist
Vol. 40, pp. 849-869 (2002)

COMPOSITION RANGES AND EXSOLUTION PAIRS FOR THE MEMBERS OF THE BISMUTHINITE–AIKINITE SERIES FROM FELBERTAL, AUSTRIA

DAN TOPA[§]

Mineralogical Institute, University of Salzburg, Hellbrunnerstrasse 34/III, A–5020 Salzburg, Austria

EMIL MAKOVICKY

Geological Institute, University of Copenhagen, Østervoldgade 10, DK–1350 Copenhagen K, Denmark

WERNER H. PAAR

Mineralogical Institute, University of Salzburg, Hellbrunnerstrasse 34/III, A–5020 Salzburg, Austria

ABSTRACT

A combination of electron-microprobe data, single-crystal X-ray diffractometry and BSE-based image analysis of polished sections was used to evaluate the composition of single-phase grains, replacement aggregates and exsolution intergrowths of the members of the bismuthinite–aikinite series from the scheelite deposit at Felbertal, Austria. Composition ranges of the classical products and new members of the series have been established, and the mineral associations in products of replacement and exsolution defined. The deposit contains a nearly complete range of bismuthinite–aikinite derivatives, the proportion of the aikinite component in them ranging from 3 to 95%. Three independent events of sulfosalt replacement were recognized at Felbertal, respectively yielding krupkaite, gladite and Cu-bearing bismuthinite as replacement products of the older bismuthinite–aikinite derivatives. Exsolution in the bismuthinite–aikinite series proceeds at each stage toward a pair of phases that are compositionally closest to the parent phase, building up to three-stage exsolution-induced sequences not described before. Ample documentation on these, as well as on all the measured compositions and crystallography of bismuthinite–aikinite derivatives, form part of this paper. We attempt a geological interpretation of the observed spatial distribution of the observed phenomena over the scale of the deposit.

Keywords: bismuthinite–aikinite derivatives, composition ranges, exsolution, replacement, miscibility gaps, scheelite deposit, Felbertal, Austria.

SOMMAIRE

Nous utilisons une combinaison de données sur la composition, obtenues avec une microsonde électronique, de données diffractométriques obtenues sur cristaux uniques, et une analyse d'images de sections polies obtenues par électrons rétrodiffusés, pour évaluer la composition de grains homogènes, d'aggrégats dus au remplacement, et de domaines en intercroissance dus à l'exsolution de membres de la série bismuthinite–aikinite dans le gisement de scheelite à Felbertal, en Autriche. Les compositions comprennent les produits classiques et de nouveaux membres des séries, et les associations de minéraux dans les produits de remplacement et d'exsolution sont définis. Le gisement contient une gamme presque complète de dérivés de la série bismuthinite–aikinite, la proportion du pôle aikinite allant de 3 à 95%. Trois événements indépendants de remplacement des sulfosels ont eu lieu à Felbertal, menant à la formation de krupkaïte, gladite et bismuthinite cuprifère, respectivement, comme produits de remplacement des dérivés de la série bismuthinite–aikinite antérieurs. L'exsolution dans la série bismuthinite–aikinite a procédé à chaque étape vers une paire de phases qui se rapprochent le plus possible du précurseur, menant à jusqu'à trois séquences dues à l'exsolution non identifiées auparavant. Nous fournissons une riche documentation sur ces produits, de même que sur toutes les compositions mesurées et sur les aspects cristallographiques des dérivés de la série bismuthinite–aikinite. Nous proposons une reconstruction géologique de la distribution des assemblages dans l'espace à l'échelle du gisement.

(Traduit par la Rédaction)

Mots-clés: dérivés de bismuthinite–aikinite, intervalles de composition, exsolution, remplacement, lacunes de miscibilité, gisement de scheelite, Felbertal, Autriche.

§ *E-mail address*: dan.topa@sbg.ac.at

INTRODUCTION

The treatment of the ordered derivatives of the bismuthinite–aikinite solid-solution series, $Cu_xPb_xBi_{2-x}S_3$ ($0 \le x \le 1$), seemed to be complete following the classical works of Ohmasa & Nowacki (1970a, b), Kohatsu & Wuensch (1971, 1976), Syneček & Hybler (1974), Mumme (1975), Horiuchi & Wuensch (1976, 1977), Mumme & Watts (1976), Mumme *et al.* (1976), and Žák (1980). Makovicky & Makovicky (1978) proposed to characterize these structures as members of the solid-solution series *aikinite* (*x*) – *bismuthinite* (100–*x*) or, in a short form, by n_{aik}, corresponding to the percentage of the $CuPbBiS_3$ end-member in the Bi_2S_3–$CuPbBiS_3$ series. The generally accepted scheme has involved three compositions, Bi_2S_3 (n_{aik} = 0, bismuthinite), $Cu_{0.5}Pb_{0.5}Bi_{1.5}S_3$ (n_{aik} = 50, krupkaite), and $CuPbBiS_3$ (n_{aik} = 100, aikinite), which have simple orthorhombic structures with "11 × 11 × 4 Å unit cells" (*i.e.*, 1*b* cell) and only one type of structural ribbons (Bi_4S_6, $CuPbBi_3S_6$ and $Cu_2Pb_2Bi_2S_6$, respectively) in each structure. These three compositions are interleaved with additional ordered structures in which ribbons of two different types combine (idealized formulae given): $CuPbBi_{11}S_{18}$ (pekoite, n_{aik} = 16.67), $CuPbBi_5S_9$ (gladite, n_{aik} = 33.33), $Cu_2Pb_2Bi_4S_9$ (hammarite, n_{aik} = 66.67), $Cu_5Pb_5Bi_7S_{18}$ (friedrichite, n_{aik} = 83.33), all these being 3*b* supercells, and $Cu_3Pb_3Bi_7S_{15}$ (lindströmite, n_{aik} = 60.0), the only phase with a 5*b* supercell.

In recent years, attention shifted to the compositional ranges of these ordered structures (*e.g.*, Harris & Chen 1976, Makovicky & Makovicky 1978, Pring 1989, Mozgova *et al.* 1990), syntheses of disordered intermediate compositions (Springer 1971, Mumme & Watts 1976), and the first annealing experiments to achieve order (Pring 1989, 1995).

New material from the metamorphosed scheelite deposit of Felbertal, Austria (Thalhammer *et al.* 1989), has substantially altered this well-established scheme. Besides yielding rich information on the compositional ranges of the established phases, it yielded, in the form of independent grains and as lamellae in exsolution pairs, three new members of the bismuthinite–aikinite series; two of these (salzburgite, $Cu_{6.4}Pb_{6.4}Bi_{25.6}S_{48}$, n_{aik} = 40, and emilite, $Cu_{10.7}Pb_{10.7}Bi_{21.3}S_{48}$, n_{aik} = 67.5) have novel, 4*b* supercells structures, and the other (paarite, $Cu_{8.5}Pb_{8.5}Bi_{31.5}S_{60}$, n_{aik} = 42.5) is a 5*b* supercell structure. The crystal-structure determinations and mineralogical descriptions of these phases are being published elsewhere (Topa *et al.* 2000, Balić-Žunić *et al.* 2002, Makovicky *et al.* 2001).

In the present contribution, concise background information about the Felbertal deposit is given, followed by a review of single, unexsolved phases and their associations. Exsolution phenomena are then treated in the order of increasing complexity: simple exsolution pairs, grains with three exsolved components and, finally, grains with four and five components observed. In the discussion, an interpretation of the observed phenomena in terms of stability and compositions of individual derivatives of bismuthinite (abbreviated as bd below) and their bearing on the conditions of formation and history of the Felbertal deposit is outlined. Only a part of extensive chemical data that form the basis of this study is published in Tables 1 and 2. Tables 3 (complete single-phase compositions), 4 (complete replacement associations), and 5 (complete exsolution assemblages) were deposited and may be obtained from the Depository of Unpublished Data, CISTI, National Research Council, Ottawa, Ontario K1A 0S2, Canada.

EXPERIMENTAL

Chemical composition

Chemical analyses were performed at the Mineralogical Institute, University of Salzburg, using a JEOL JXA–8600 electron microprobe, controlled by a LINK–*eXL* system, operated at 25 kV, and 30 nA, 20 s counting time for peaks and 7 s for background. Under these conditions, the expected diameter of the beam, ~0.5 μm, was slightly defocused (to ~2 μm) to prevent damage to the sample. The expected spatial resolution for the matrix of bismuthinite derivatives (ρ ~7 g cm^{-3}) is ~3 μm. The following natural (n) and synthetic (s) standards and X-ray lines were used: n-$CuFeS_2$ (Cu*K*α, Fe*K*α), s-Bi_2S_3 (Bi*L*α, S*K*α), n-PbS (Pb*L*α), s-CdTe (Cd*L*β, Te*L*α), n-Sb_2S_3 (Sb*L*α) and pure metal for Ag*L*α. The raw data were corrected with the on-line ZAF–4 procedure. Standard deviations (error in wt.%) of elements sought for the matrix of bismuthinite derivatives (in the gladite–krupkaite range) are: Bi 0.17, Pb 0.1, Cu and Sb 0.03, Fe 0.01 and S 0.06%. The other elements are below 3σ detection limit: Ag 0.07, Te 0.08 and Cd 0.17 wt.%. Results of three to five point-analyses obtained from a homogeneous grain or individual exsolved phase were averaged. These mean compositions are compiled in Tables 1 and 2 and used in Figures 2 to 13. Some grains contain traces of Sb (less than 0.3 wt.%), and others, traces of Fe (less than 0.12 wt.%). Empirical formulae $Cu_xPb_yBi_{8-½(x+y)}S_{12}$ ($x = y$ for ideal compositions) were calculated for all grains and exsolution lamellae on the basis (Cu + Pb)/2 + Bi = 8 atoms per formula unit, *apfu*, after Makovicky & Makovicky (1978). The position of these phases in the bismuthinite–aikinite series is described by the hypothetical percentage of the aikinite end-member $n_{aik} = 25(x + y)/2$. The value of $\Delta n_{aik} = \pm 12.5(y - x)$ is used to express the accuracy of the analytical data.

BSE imaging and image analysis

Valuable information was obtained on compositional differences of bismuthinite derivatives and associated phases by using back-scattered electron (BSE) signals. The contrast in BSE images is related to the mean

atomic number z_m of a compound, defined as $(\Sigma c_i z_i)/100$, where c_i and z_i are concentrations in wt.% and atomic numbers for Cu, Pb, Bi and S, in case of a bismuthinite derivatives. The resolution of a modern BSE detector with respect to atomic numbers is less than $\Delta z_m = 0.1$. Bismuthinite derivatives, in the bismuthinite–aikinite range, have mean atomic numbers ranging from 70.47 for Bi_2S_3 to 65.49 for $CuPbBiS_3$. Any two phases in that range, separated by a 2% difference in the n_{aik} value, will have slightly different mean atomic numbers [$\Delta z_m > 0.1$], and consequently can be imaged.

BSE images with 200- to 1000-fold magnifications were acquired digitally in Slow Kalman mode (about 15 frames for each image in order to obtain noise reduction) at 25 kV accelerating voltage and 10 nA beam current under control of the LINK–*eXL* software. A typical BSE image of exsolution lamellae of bismuthinite derivatives shows two or more phases (with different z_m) with different levels of grey (the brighter phase contains less Cu and Pb than the darker phase).

A LINK Image Phase Analysis package was used to calculate the relative area of phases present in each image based on the distribution of pixel intensities (1024 × 1024 pixels). The area percentage and composition of each phase are used to estimate the initial composition of exsolved grains.

Single-crystal X-ray diffraction

The chemical analyses were supplemented by single-crystal X-ray diffraction of all suitable single-phase grains extracted from the quartz matrix using HF and mechanical means. Only the grains exactly characterized by electron-microprobe analyses were used.

The crystal fragments, with irregular shapes and <0.1 mm in diameter, were measured on a Bruker AXS four-circle diffractometer equipped with CCD 1000K area detector (6.25 × 6.25 cm active detection area, 512 × 512 pixels) and a flat graphite monochromator using Mo*K*α radiation from a fine-focus sealed X-ray tube. The sample–detector distance was generally 6 cm, but a greater distance was used for the cases with large superperiods. For some fragments, complete determination of the crystal structure was performed (to be reported elsewhere), resulting in data on the unit cell and space group; in cases of less suitable material, only the superstructure periodicity was determined. These data, supplemented by a small amount of data on bd from other localities (Zirknitzstollen and Sedl, Tauern Window, Austria; Băiţa Bihor, Romania; Outlaw mine, Nevada, U.S.A.) are summarized in Table 1 and give the most complete picture of bd mineralogy to date. The SMART system of programs was used for unit-cell determination and data collection, SAINT+ for the calculation of integrated intensities, and SHELXTL for the structure solution and refinement (all Bruker AXS products).

Geology and Mineralogy of Felbertal

The Felbertal scheelite deposit is one of the largest tungsten mines in operation. The deposit has produced more than 7×10^6 t of ore. Its current production is 4×10^5 t/yr at an ore grade of 0.5% WO_3. The scheelite ore is hosted by a Cambro-Ordovician volcanic arc sequence (metabasalts, metagabbros and orthogneisses) and Variscan granites (Fig. 1). The latter belong to an early episode (340 Ma) of a multi-stage cycle of Variscan magmatic activity (Eichhorn *et al.* 2000). Economically significant scheelite orebodies are assumed to be genetically associated with the Variscan K1–K3 granitic plutons (Raith *et al.* 2001).

The deposit consists of two parts, denoted locally as ore fields; it is situated within a sequence up to 400 m thick that is considered to represent stacked nappes (Ebner *et al.* 2000). The Western Ore Field comprises two ore-bearing wedges separated by barren paragneiss and micaschist (Fig. 1). Several distinct orebodies (K1–K8) of this field are mined underground. The orebodies dip steeply (on average at 45° in the SSE–NNW profile), each of them spanning a range of absolute heights above the sea level. The Westfeld profile (Fig. 1b) is perpendicular to this dip. The Eastern Ore Field was mined by open-pit methods and is abandoned now.

Three different generations of scheelite are distinguished (Höll 1975). The first two represent yellowish-fluorescent Mo-bearing scheelite, whereas the third is a remobilized bluish-fluorescent scheelite. Scheelite may be associated with beryl, phenakite and chrysoberyl, fluorite, as well as with a variety of sulfides and sulfosalts. The dominant sulfides are pyrrhotite, pyrite, chalcopyrite (± stannite, sphalerite), and intermediate members of the molybdenite–tungstenite solid solution (from WS_2 to $W_{0.9}Mo_{0.1}S_2$). These occur as finely dispersed flakes in the generations of greyish scheelite and as local concentrations within the orebodies. Trace amounts of arsenopyrite, pentlandite, marcasite, cobaltite, enargite, tennantite–tetrahedrite, stibnite, galena, cassiterite, columbite and ferberite are present as well (Höll 1975).

The sulfosalt accumulations occur as (1) lens-shaped massive accumulations in bodies of quartz, (2) fine layers in laminated and discordant quartz veins in amphibolites, and (3) irregular distributions in quartz stringers and veinlets of the scheelite ore. There is an abundance of galenobismutite, cosalite, bismuthinite derivatives, members of the lillianite, pavonite, junoite and cuprobismutite homologous series, cannizzarite, eclarite, as well as tetradymite, joséite-B, hessite and native bismuth. Small amounts of microscopic native gold may accompany the sulfosalts.

Both syngenetic and epigenetic models have been proposed for the genesis of this deposit. The concepts range from sedimentary-exhalative processes for the tungsten enrichment (Eichhorn *et al.* 1999) to epigenetic

TABLE 1. CHEMICAL COMPOSITION AND CRYSTAL DATA FOR BISMUTHINITE–AIKINITE DERIVATIVES FROM FELBERTAL, AUSTRIA

Sample	*n*	Cu	Fe	Pb	Bi	Sb	S	Total	n_{aik}	Δn_{aik}	ev	Cu	Pb	Bi	S	*a* (Å)	*b* (Å)	*c* (Å)	S.G.	mineral
Bi_2S_3 synthetic		0.00	0.00	0.00	81.29	0.00	18.71	100.00	0.0	0.0	0.00	0.00	0.00	8.00	12.00	3.9853(4)	11.163(1) = 1×11.163	11.314(1)	*Pmcn*	*bismuthinite*
Zirknitzstollen	23	1.24(3)	0.00	4.4(1)	76.2(4)	0.00	18.69(8)	100.5(4)	10.5	0.4	–0.95	0.40	0.44	7.58	12.12		1-fold		ortho.*P*	bismuthinite
FE-88/2-1-6	10	1.23(2)	0.00	4.4(1)	75.8(2)	0.12(2)	18.52(7)	100.1(3)	10.6	0.6	–0.21	0.40	0.45	7.58	12.04	3.991(1)	11.187(3) = 1 × 11.187	11.337(3)	*Pmcn*	bismuthinite
FE-88/2-1-12	5	1.49(1)	0.00	5.5(5)	74.4(1)	0.12(1)	18.23(6)	99.7(1)	13.1	0.8	0.84	0.49	0.55	7.48	11.92		?		?	?
FE-88/2-1-7	12	1.89(8)	0.00	6.8(2)	72.4(4)	0.12(2)	18.2(2)	99.5(1)	16.5	0.8	0.04	0.63	0.69	7.34	12.01	3.9884(3)	33.454(3) = 3 × 11.151	11.363(1)	$Pmc2_1$	*pekoite**
FE-88/2-1-8	10	2.07(7)	0.00	7.4(1)	71.7(4)	0.12(2)	18.3(1)	99.5(3)	18.0	0.8	–0.21	0.69	0.75	7.28	12.04	3.983(1)	33.43(1) = 3 × 11.142	11.318(4)	$Pmc2_1$	pekoite*
FE-97/3B-50	5	3.84(3)	0.05(1)	13.4(1)	64.3(1)	0.00	17.88(4)	99.5(1)	33.7	0.6	–0.12	1.32	1.37	6.65	12.03	4.0044(4)	33.575(3) = 3 × 11.192	11.480(1)	*Pmcn*	*gladite*
FE-97/3-sg6	5	3.97(6)	0.04(1)	13.5(1)	64.7(2)	0.00	18.34(6)	100.6(2)	34.1	0.3	–1.76	1.35	1.38	6.64	12.22		3-fold		ortho.*P*	gladite
FE-97/3B-10	6	4.31(1)	0.10(1)	15.3(1)	63.0(2)	0.00	18.03(7)	100.7(2)	37.8	0.6	–0.17	1.49	1.54	6.49	12.03		3-fold		ortho.*P*	gladite
FE-97/3a-37	6	4.36(3)	0.07(1)	15.4(1)	62.9(1)	0.00	17.94(7)	100.7(1)	38.2	0.8	0.38	1.50	1.56	6.47	11.97		3-fold		ortho.*P*	gladite
FE-97/3A1-63	12	4.59(5)	0.00	15.3(1)	62.7(2)	0.00	17.98(3)	100.6(3)	39.2	0.5	–0.04	1.55	1.59	6.43	12.02	4.0100(3)	33.589(3) = 3 × 11.196	11.502(1)	*Pmcn*	gladite
FE-97/3b-21	5	4.65(4)	0.05(1)	16.0(1)	61.6(1)	0.00	17.79(4)	100.0(1)	40.5	0.6	0.33	1.60	1.64	6.38	11.97	4.0074(9)	44.81(1) = 4 × 11.203	11.513(3)	$Pmc2_1$	salzburgite
FE-97/3-"bd27"	20	4.72(5)	0.06(1)	16.3(1)	61.5(3)	0.00	17.90(7)	100.5(2)	41.1	0.6	0.08	1.62	1.67	6.35	12.00	4.011(1)	44.81(1) = 4 × 11.203	11.522(3)	$Pmc2_1$	salzburgite
FE-97/3-sg56	5	4.79(3)	0.08(1)	16.7(1)	60.9(2)	0.00	17.83(4)	100.3(2)	42.1	0.7	0.21	1.66	1.71	6.32	11.99	4.0070(6)	55.998(8) = 5 × 11.200	11.512(2)	*Pmcn*	*paarite*
FE-97/3-sg62	7	4.85(4)	0.08(1)	16.7(2)	60.4(5)	0.00	17.87(8)	99.8(3)	42.6	0.4	–0.66	1.69	1.72	6.30	12.09		3- and 5-fold			exsolved
FE-97/3A1-31	5	5.36(4)	0.00	18.1(1)	58.2(1)	0.07(1)	17.63(5)	99.6(2)	47.1	0.9	–0.37	1.85	1.92	6.12	12.06	4.0134(4)	11.208(1) = 1 × 11.207	11.560(1)	$Pmc2_1$	krupkaite
FE-97/3a-7'	3	5.51(5)	0.00	18.3(2)	58.8(1)	0.00	17.76(3)	100.4(2)	47.5	0.5	0.00	1.88	1.92	6.10	12.01		1-fold		ortho.*P*	krupkaite
FE-97/3B-14	4	5.82(5)	0.00	19.3(1)	57.3(2)	0.10(1)	17.78(8)	100.3(3)	50.3	0.4	–0.25	2.00	2.03	5.99	12.04	4.0145(4)	11.202(1) = 1 × 11.202	11.560(1)	$Pmc2_1$	*krupkaite*
FE-86/k7-3-30	4	6.45(5)	0.00	21.7(1)	54.0(1)	0.09(1)	17.7(1)	99.9(2)	56.8	0.7	–0.33	2.24	2.30	5.73	12.05		1-fold		ortho.*P*	krupkaite
FE-86/k7-2-12	6	6.65(9)	0.00	22.4(3)	53.2(5)	0.00	17.60(6)	99.9(3)	59.0	1.0	–1.19	2.32	2.40	5.64	12.16	4.0212(5)	11.232(1) = 1 × 11.232	11.581(1)	$Pmc2_1$	krupkaite
FE-89/9-sg33	5	6.75(3)	0.06(1)	23.0(1)	52.7(1)	0.12(2)	17.52(6)	100.1(2)	59.9	0.7	–0.33	2.37	2.42	5.60	12.06		5-fold		ortho.*P*	lindströmite
FE-86/k7-3-28	12	6.85(4)	0.00	22.8(1)	52.8(1)	0.09(1)	17.5(1)	100.1(2)	60.1	0.7	–0.21	2.38	2.43	5.59	12.04	4.0179(3)	56.141(4) = 5 × 11.228	11.578(1)	*Pmcn*	*lindströmite**
FE-86/k7-2-6	7	7.06(7)	0.00	23.5(1)	51.8(4)	0.00	17.6(1)	99.9(5)	62.4	0.7	–1.23	2.47	2.52	5.50	12.16		5-fold		ortho.*P*	lindströmite
FE-86/k7-2-5	7	7.23(5)	0.00	24.2(1)	51.1(5)	0.00	17.53(7)	100.1(5)	64.1	0.9	–1.07	2.53	2.60	5.44	12.15	4.0206(4)	56.147(5) = 5 × 11.229	11.586(1)	*Pmcn*	lindströmite*
FE-86/k7-2-7	7	7.49(5)	0.00	24.9(1)	50.1(3)	0.00	17.48(9)	100.0(5)	66.4	0.7	–1.15	2.63	2.68	5.34	12.15	4.026(2)	44.97(2) = 4 × 11.242	11.614(5)	$Pmc2_1$	emilite
FE-86/K7-sg9c	5	7.68(3)	0.00	25.4(1)	49.9(1)	0.00	17.59(4)	100.6(1)	67.5	0.5	–1.36	2.68	2.72	5.30	12.18	4.0285(5)	44.986(9) = 4 × 11.247	11.599(2)	$Pmc2_1$	emilite
FE-86/k7-4-36	5	7.62(4)	0.00	25.8(1)	49.4(2)	0.00	17.6(1)	100.4(3)	68.1	1.3	–1.51	2.67	2.78	5.28	12.21	4.0248(5)	33.773(4) = 3 × 11.258	11.595(1)	*Pmcn*	*hammarite*
FE-86/k7-2-20	7	7.67(4)	0.00	25.6(1)	49.1(1)	0.00	17.44(8)	99.9(2)	68.4	0.9	–1.31	2.70	2.77	5.26	12.18		3-fold		ortho.*P*	hammarite
FE-89/7-36	11	8.09(2)	0.00	26.9(1)	47.5(2)	0.22(7)	16.93(4)	99.7(3)	71.9	0.8	1.74	2.85	2.91	5.12	11.81		3-fold		ortho.*P*	hammarite
FE-86/k7-8-53	5	8.21(5)	0.00	27.0(2)	47.5(3)	0.08(1)	16.83(9)	99.5(2)	72.6	0.3	2.13	2.89	2.92	5.10	11.75	4.0293(7)	33.800(6) = 3 × 11.266	11.604(2)	*Pmcn*	hammarite
FE-89/9-3-19d	5	8.25(7)	0.00	27.7(2)	46.7(3)	0.07(1)	17.4(2)	100.1(4)	74.0	1.2	–1.23	2.92	3.01	5.04	12.18		?		?	?
FE-89/9-1-49h	4	8.69(4)	0.00	28.8(1)	45.1(1)	0.09(1)	16.94(3)	99.6(1)	77.8	0.6	0.63	3.09	3.14	4.89	11.94		?		?	?
FE-89/7-38	5	8.92(2)	0.00	29.9(1)	44.3(2)	0.40(3)	16.9(1)	100.5(2)	79.6	1.1	1.43	3.14	3.23	4.82	11.85	4.0324(6)	33.858(2) = 3 × 11.286	11.609(2)	$Pmc2_1$	*friedrichite*
Sedl	40	8.94(6)	0.00	29.5(3)	44.5(1)	0.00	17.06(7)	100.0(3)	79.9	0.5	0.00	3.18	3.22	4.80	12.01	4.0343(7)	33.891(6) = 3 × 11.297	11.621(2)	$Pmc2_1$	*friedrichite*
Outlaw mine	25	9.29(9)	0.00	30.7(3)	43.6(4)	0.00	17.14(7)	100.7(2)	82.7	0.5	–0.12	3.29	3.33	4.69	12.03		1-fold		ortho.*P*	aikinite
Baiţa Bihor	4	9.35(5)	0.00	30.6(1)	43.1(1)	0.15(2)	17.01(4)	100.2(2)	83.1	0.2	0.38	3.32	3.33	4.67	11.96	4.0346(7)	11.296(2) = 1 × 11.296	11.635(2)	*Pmcn*	aikinite
FE-89/9-2-G32	6	9.31(4)	0.00	31.3(2)	42.3(2)	0.00	17.0(2)	99.9(3)	84.8	1.3	–0.62	3.34	3.44	4.61	12.10	4.0404(6)	11.316(2) = 1 × 11.316	11.637(2)	*Pmcn*	aikinite
Baiţa Bihor	4	9.77(4)	0.00	32.0(2)	41.4(2)	0.00	16.95(9)	100.2(2)	87.5	0.2	0.00	3.49	3.51	4.50	12.00		1-fold		ortho.*P*	aikinite
FE-89/9-sg6a	4	9.75(8)	0.00	32.7(3)	41.6(3)	0.00	16.89(7)	100.9(2)	87.7	1.2	1.14	3.46	3.56	4.49	11.89		1-fold		ortho.*P*	aikinite
FE-89/9-1-54	5	10.14(5)	0.00	33.7(2)	39.0(1)	0.00	16.65(2)	99.6(2)	92.6	0.9	0.67	3.67	3.74	4.29	11.94	4.0422(6)	11.339(2) = 1 × 11.339	11.652(2)	*Pmcn*	aikinite
FE-89/9-2-7	5	10.36(7)	0.00	34.5(1)	38.4(3)	0.00	16.8(1)	100.0(2)	94.6	0.9	–0.25	3.75	3.82	4.22	12.05		1-fold		ortho.*P*	aikinite

Notes: *n* is the number of analyses made. Values in parentheses signify one standard deviation in terms of the last digit. The compositions are expressed in terms of weight % constituents, then recast as empitrical formulae. n_{aik}, Δn_{aik} and the empirical formulae are calculated according to the rules given in the text; ev (%) is 100*(Σcation charge – Σanion charge)/Σanion charge. Asterisks denote presence of X-ray-detected exsolution phenomena in the crystal analyzed. We were not able to distinguish two phases by electron-microprobe analysis in the case of lindströmite. Italics denote a phase very close to its ideal composition. No structural information could be obtained from grains denoted by ?. Additional localities are specified in the text. S.G.: space group.

granite-related models (Briegleb 1991). Recent Re–Os dating of molybdenite associated with scheelite and sulfosalts from the K1 and K2 orebodies revealed a main ore-forming event at 340–345 Ma (Raith *et al.* 2001), suggesting its genetic link with the early Carboniferous magmatic activity. On the basis of textural relationships, the sulfosalt mineralization postdates the crystallization of molybdenite and is also considered a result of the polyphase Variscan magmatic events. Subsequently, the entire mass of rock and ore was subjected to the Alpine prograde metamorphism of the upper greenschist to lower amphibolite facies (500–590°C and 4.5–7 kbar; Eichhorn 1995), followed by retrograde recrystallization.

Single Phases

In most cases, bismuthinite derivatives (bd) in the Felbertal deposit form sulfosalt grains in a quartz gangue; usually these are intergrowths of two or more sulfosalts. Besides one or two distinct bd (homogeneous or exsolved), the aggregates may contain a member of the lillianite homologous series (lillianite–gustavite solid solution, vikingite, heyrovskyite), a member of the pavonite homologous series (makovickyite, pavonite), junoite, felbertalite (Topa *et al.* 2001), cannizzarite or a member of the cuprobismutite homologous series [cuprobismutite, hodrushite, kupčíkite $Cu_{3.4}Fe_{0.6}Bi_5S_{10}$ (Topa *et al.* in prep.)], in addition to some later products of decomposition (especially native Bi).

The total amount of empirical data on single-phase bd from Felbertal (Table 3, deposited) yields a quasi-continuous series of compositions with only two obvious compositional gaps, between pekoite (bd_{18}) and gladite (bd_{33}) and between krupkaite (bd_{47}) and the members with $n_{aik} < 43$, respectively (Fig. 2). Neither the ideal aikinite, $CuPbBiS_3$, nor the ideal bismuthinite, Bi_2S_3, are reached, the respective limits found being $n_{aik} = 95$ and $n_{aik} = 3$.

As indicated in Table 1, bismuthinite (1-fold structure), gladite (3-fold superstructure), krupkaite (1-fold structure), hammarite (3-fold superstructure) and aikinite (1-fold structure) show appreciable compositional ranges. Salzburgite (4-fold superstructure),

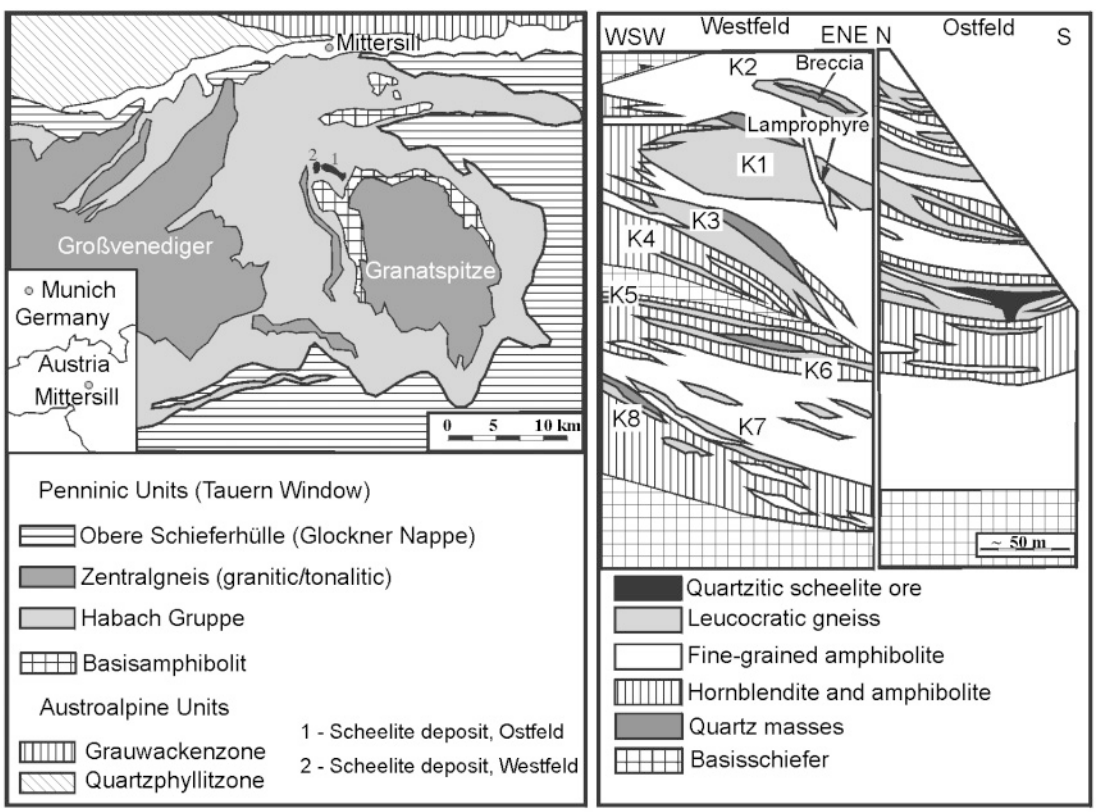

FIG. 1. a) Schematic geological map of the central part of the Tauern Window (the Eastern Alps), with the position of the Felbertal ore fields indicated. b) Simplified geological profiles of the western and eastern parts of the Felbertal ore fields.

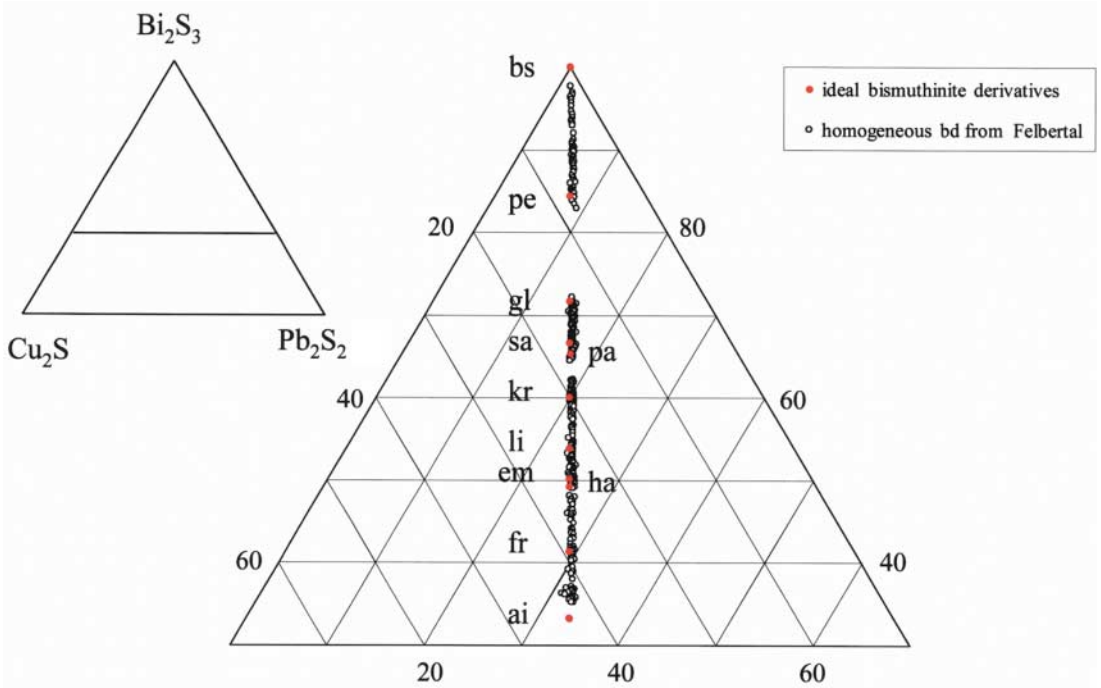

FIG. 2. Empirical compositions of bismuthinite derivatives from Felbertal, with the ideal compositions of known minerals and new, crystallographically characterized phases (salzburgite, paarite and emilite). Molar percentages as indicated. Abbreviations used throughout the text: bs: bismuthinite, pe: pekoite, gl: gladite, sa: salzburgite, pa: paarite, kr: krupkaite, li: lindströmite, em: emilite, ha: hammarite, fr: friedrichite, ai: aikinite, and bd_{naik}: bismuthinite derivatives with the percentage of aikinite end-member equal to n_{aik}.

friedrichite (3-fold superstructure) as well as the new phases paarite (5-fold superstructure) and emilite (4-fold superstructure) have narrow compositions and also narrow compositional gaps with respect to the adjacent, crystallographically distinct phases. The width of the lindströmite and pekoite fields is less certain because both appear to be analytically inseparable components of nearly submicroscopic exsolution-induced intergrowths, respectively, with krupkaite and bismuthinite.

REPLACEMENT PAIRS

Ore textures of a number of small aggregates of sulfosalts enclosed in quartz (or sulfides) indicate that not all bd (and not all sulfosalts) crystallized at the same time, in one pulse of ore formation. Where possible, we note that the late phase is poorer in Cu–Pb, *i.e.*, with a lower n_{aik} value, than the earlier one. What is typical in these intergrowths is partial replacement, either along well-defined boundaries or with a broad transitional zone, implying a partial alteration of the former phase. In these cases, exsolution textures probably develop in the transition zone between the cores or last remnants of the original phase and the rims or fingers of the new phase. The replacement textures (Fig. 3) and the coexisting pairs (Fig. 4) suggest non-equilibrium associations, with the difference in respective n_{aik} values ranging from less pronounced (*e.g.*, for the association Cu-bearing bismuthinite – gladite) *via* intermediate values (*e.g.*, bismuthinite–krupkaite) to the extreme cases, such as at the contact of Cu-bearing bismuthinite with aikinite. Only in rare instances, typified by the pairs krupkaite–gladite, krupkaite–salzburgite and lindströmite–krupkaite, might the coexistence of two bd phases represent an equilibrium assemblage. The first of these pairs, krupkaite–gladite, seems to be especially common.

FIG. 3. Typical examples of replacement associations of two-to-three bismuthinite derivatives. a–c: Replacement along cleavage planes. b,d,f: Replacement from the margins. Two-step replacements are in (c) and (e); post-replacement exsolution took place in the reaction zone in (f). EMP data are provided in Table 2. Associated phases: bd: bismuthinite derivatives, gb: galenobismutite, ^{4}L: lillianite, ^{4}P: makovickyite, ^{5}P: pavonite, ca: cannizzarite, co: cosalite, ku: kupčíkite, bi: native bismuth.

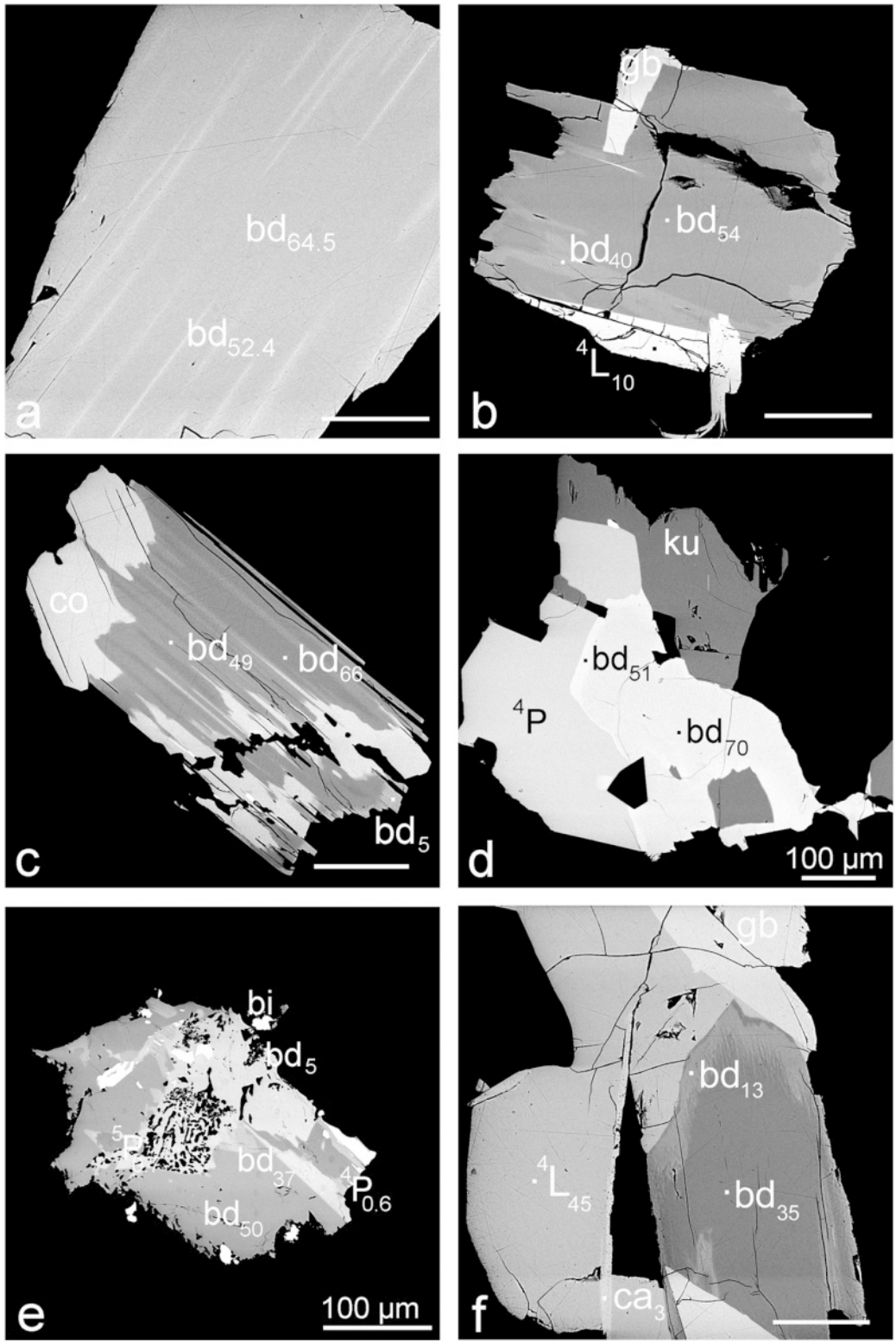
a
bd64.5
bd52.4
b
gb
bd54
bd40
4L10
c
co
bd49
bd66
bd5
d
ku
bd51
4P
bd70
100 µm
e
bi
bd5
5P
bd37
4P0.6
bd50
100 µm
f
gb
bd13
4L45
bd35
ca3

TABLE 2. ANALYTICAL DATA FOR SELECTED REPLACEMENT ASSOCIATIONS AND EXSOLUTION PAIRS IN THE FELBERTAL DEPOSIT, AS ILLUSTRATED IN FIGURES 3-13

Sample	Fig.	Cu	Fe	Pb	Bi	Sb	S	Total	n_{atk}	Δn_{atk}	ev	Pb/Cu	Cu	Pb	Bi	S	area %	BD
FE-86/K7-1-gr15-d'. m	3a	5.93	0.00	20.2	55.8	0.00	17.39	99.3	52.7	1.1	0.4	1.04	2.06	2.15	5.89	11.97	–	–
FE-86/K7-1-gr15-d.. m	3a	7.23	0.00	24.4	50.8	0.01	17.35	99.7	64.5	1.1	–0.4	1.03	2.54	2.62	5.42	12.07	–	–
Fe-86/k7-7-G44m.... m	3b	4.54	0.04	16.2	61.4	0.07	18.27	100.6	40.4	1.5	–2.4	1.08	1.56	1.68	6.38	12.32	–	–
Fe-86/k7-7-G44d..... m	3b	5.94	0.08	21.2	54.8	0.08	18.05	100.2	54.0	1.6	–3.1	1.06	2.10	2.23	5.84	12.42	–	–
FE-89/9-sg24b-h..... m	3c	0.61	0.00	2.2	78.7	0.22	19.07	100.7	5.2	0.2	–2.0	1.08	0.20	0.21	7.79	12.26	–	–
FE-89/9-sg24b-m..... m	3c	5.62	0.00	19.1	57.8	0.14	17.87	100.5	49.1	1.0	–0.8	1.04	1.92	2.00	6.04	12.12	–	–
FE-89/9-sg24b-d..... m	3c	7.36	0.00	25.0	50.0	0.08	17.57	100.0	66.0	1.4	–1.8	1.04	2.59	2.70	5.36	12.24	–	–
FE-89/9-sg14-m'..... m	3d	5.75	0.11	20.1	56.8	0.00	17.74	100.5	51.1	0.8	–0.2	1.03	2.01	2.07	5.96	12.04	–	–
FE-89/9-sg14-m..... m	3d	7.80	0.05	26.8	48.3	0.00	17.46	100.4	70.4	1.3	–1.1	1.04	2.76	2.87	5.19	12.16	–	–
FE-89/9-D-h..... m	3e	0.46	0.00	2.8	77.6	0.11	18.59	99.5	5.4	1.6	–0.8	1.84	0.15	0.28	7.78	12.13	–	–
FE-89/9-D-m..... m	3e	4.39	0.00	14.6	64.1	0.00	17.99	101.1	37.1	0.4	0.8	1.02	1.47	1.50	6.52	11.92	–	–
FE-89/9-D-d..... m	3e	5.70	0.00	19.2	57.1	0.00	17.67	99.8	50.1	0.9	–0.6	1.04	1.97	2.04	6.00	12.09	–	–
FE-86/K7-1-gr17-d'. m	3f	1.49	0.00	5.5	74.4	0.12	18.23	99.7	13.1	0.8	0.8	1.13	0.49	0.55	7.48	11.92	–	–
FE-86/K7-1-gr17-d...m	3f	3.95	0.09	14.3	63.8	0.00	18.03	100.2	35.2	1.0	–0.5	1.06	1.37	1.45	6.59	12.07	–	–
FE-97/3-sg109c-mtr. m	5a	4.49	0.00	15.0	62.4	0.00	17.76	99.6	38.7	0.5	0.3	1.03	1.53	1.57	6.45	11.97	85.6	40.2
FE-97/3-sg109c-ld... m	5a	5.68	0.00	19.1	58.1	0.00	17.46	100.3	49.2	0.7	1.7	1.03	1.94	2.00	6.03	11.81	14.4	
Fe-97/3a-gr32C-ld... m	5b	4.85	0.00	16.1	60.8	0.00	17.77	99.5	41.9	0.4	–0.4	1.02	1.66	1.69	6.32	12.05	50.8	40.4
Fe-97/3a-gr32C-lh... m	5b	4.53	0.00	15.3	63.0	0.00	17.91	100.7	38.8	0.7	0.6	1.04	1.53	1.58	6.45	11.94	49.2	
FE-97/3Bgr3-mtrd.... m	5c	4.77	0.00	15.8	61.9	0.00	18.11	100.6	40.7	0.3	–1.2	1.01	1.62	1.64	6.37	12.15	91.0	40.5
FE-97/3Bgr3-lh..... m	5c	4.50	0.00	14.9	62.9	0.00	17.92	100.2	38.4	0.3	0.0	1.02	1.52	1.55	6.46	12.01	9.0	
FE-97/3a-23h..... m	5d	4.54	0.00	15.2	63.0	0.00	17.92	100.6	38.7	0.5	0.4	1.02	1.53	1.57	6.45	11.96	14.5	41.5
FE-97/3a-23matr..... m	5d	4.92	0.00	16.4	61.6	0.00	17.80	100.8	42.0	0.5	0.9	1.03	1.66	1.70	6.32	11.90	85.5	
FE-97/3bgrs-mtrh.... m	5e	4.70	0.07	16.4	61.2	0.00	18.01	100.3	41.3	0.6	–1.0	1.03	1.63	1.68	6.35	12.13	91.1	41.8
FE-97/3bgrs-ld..... m	5e	5.37	0.05	18.0	58.5	0.03	17.59	99.5	46.7	0.1	0.3	1.00	1.87	1.87	6.13	11.96	8.9	
FExx-23-lh..... m	5f	4.34	0.09	15.2	62.4	0.26	17.58	99.9	38.0	0.5	2.3	1.03	1.50	1.54	6.48	11.75	47.5	43.2
FExx-23-ld..... m	5f	5.53	0.00	18.6	58.3	0.16	17.31	99.8	47.9	0.7	2.5	1.03	1.89	1.94	6.08	11.73	52.5	
FE-97/3-sg104a-h.. m	5g	4.86	0.00	16.4	60.5	0.00	17.60	99.4	42.3	0.7	0.5	1.04	1.67	1.72	6.30	11.96	75.5	43.8
FE-97/3-sg104a-d.. m	5g	5.55	0.00	18.6	58.0	0.00	17.48	99.6	48.4	0.7	0.8	1.03	1.91	1.96	6.06	11.92	24.5	
FE-97/3-sg102a-h.. m	5h	4.43	0.00	15.0	62.4	0.00	17.75	99.6	38.5	0.7	0.3	1.04	1.51	1.57	6.46	11.97	25.8	45.9
FE-97/3-sg102a-d.. m	5h	5.57	0.04	18.7	57.8	0.00	17.60	99.7	48.5	0.2	0.1	1.01	1.93	1.95	6.06	11.99	74.3	
Fe-97/3P19b-lh..... m	5i	4.61	0.00	15.6	61.5	0.00	17.84	99.6	40.1	0.7	–0.6	1.04	1.58	1.63	6.40	12.09	25.0	46.5
Fe-97/3P19b-ld..... m	5i	5.51	0.00	18.8	57.9	0.00	17.63	99.9	48.6	1.1	0.0	1.05	1.90	1.99	6.06	12.02	75.0	
FE-97/3bgru-h..... m	5j	4.98	0.00	16.7	60.6	0.12	18.02	100.4	42.9	0.7	–1.0	1.03	1.69	1.74	6.28	12.14	6.5	46.4
FE-97/3bgru-d..... m	5j	5.36	0.00	17.7	58.5	0.00	17.66	99.3	46.6	0.4	–0.5	1.02	1.85	1.88	6.14	12.07	93.5	
Fe-97/3-D-gr49-lh... m	5k	4.64	0.00	15.9	61.6	0.00	17.92	100.1	40.4	1.0	–0.6	1.05	1.58	1.66	6.38	12.09	15.1	45.7
Fe-97/3-D-gr49-ld... m	5k	5.55	0.00	18.6	57.9	0.00	17.69	99.9	48.5	0.7	–0.5	1.03	1.91	1.97	6.06	12.07	9.3	
Fe-97/3-D-gr49-mtr. m	5k	5.33	0.00	17.8	58.6	0.00	17.58	99.3	46.4	0.6	0.0	1.03	1.84	1.89	6.14	12.01	75.6	
Fe-97/3B-gr52-lh..... m	5l	4.18	0.07	15.0	62.8	0.00	17.83	99.8	37.3	1.1	0.2	1.06	1.45	1.53	6.51	12.00	–	–
Fe-97/3B-gr52-mtr.. m	5l	4.41	0.06	15.6	62.0	0.00	17.90	100.0	39.1	1.0	–0.4	1.05	1.52	1.60	6.44	12.07	–	–
Fe-97/3B-gr52-ld1... m	5l	4.53	0.06	15.8	62.0	0.00	18.12	100.6	39.7	0.8	–1.2	1.04	1.56	1.62	6.41	12.16	–	–
Fe-97/3B-gr52-ld2... m	5l	4.80	0.00	16.4	60.6	0.00	17.82	99.7	42.1	1.0	–0.6	1.05	1.65	1.72	6.32	12.09	–	–
Fe-97/3B-gr52-lsd... m	5l	5.52	0.00	18.6	58.1	0.00	17.41	99.6	48.2	0.7	1.4	1.03	1.90	1.96	6.07	11.85	–	–
FE-97/3-sg40a-ld..... m	7a	1.08	0.01	3.8	76.2	0.00	18.47	99.6	9.2	0.3	–0.3	1.06	0.36	0.38	7.63	12.04	39.6	24.0
FE-97/3-sg40a-ld..... m	7a	3.87	0.07	13.4	64.3	0.00	17.90	99.5	33.7	0.3	–0.1	1.02	1.34	1.36	6.65	12.02	60.4	
FE-97/3-sg47-lh..... m	7b	1.33	0.00	4.5	74.9	0.07	18.64	99.4	11.2	0.2	–1.9	1.03	0.44	0.46	7.55	12.23	25.7	28.0
FE-97/3-sg47-mtr... m	7b	3.85	0.07	13.5	64.2	0.05	18.06	99.8	33.8	0.6	–0.9	1.04	1.33	1.38	6.65	12.12	74.3	
Fe-97/3-D-gr25-lh... m	7c	1.88	0.00	6.5	72.9	0.00	18.23	99.6	16.1	0.5	0.2	1.06	0.62	0.66	7.36	11.98	16.9	30.8
Fe-97/3-D-gr25-mtr. m	7c	3.84	0.00	13.1	64.3	0.00	18.02	99.3	33.5	0.8	–1.2	1.05	1.31	1.37	6.66	12.17	83.1	
Fe-97/3-D-gr56-lh... m	7d	1.82	0.00	6.4	73.0	0.00	18.21	99.9	15.7	0.6	0.2	1.08	0.60	0.65	7.37	11.99	7.3	32.9
Fe-97/3-D-gr56-mtr. m	7d	3.89	0.00	13.6	64.2	0.00	17.81	99.5	34.2	1.2	0.2	1.07	1.32	1.42	6.63	12.00	92.7	
Fe-97/3a-gr32c-lh... m	9a	4.50	0.00	15.1	62.5	0.00	17.79	99.9	38.8	0.6	0.4	1.03	1.53	1.57	6.45	11.96	–	–
Fe-97/3a-gr32c-lm.. m	9a	4.87	0.00	16.4	61.0	0.00	17.79	100.1	42.2	0.7	0.1	1.03	1.66	1.72	6.31	12.00	–	–
Fe-97/3a-gr32c-d... m	9a	5.67	0.00	18.8	58.4	0.00	17.88	100.7	48.6	0.4	–0.5	1.02	1.93	1.96	6.05	12.07	–	–
Fe-97/3B-gr6-lm..... m	9b	4.47	0.06	16.1	61.2	0.00	17.69	99.4	40.2	1.4	0.2	1.07	1.55	1.66	6.39	12.01	–	–
Fe-97/3B-gr6-lh..... m	9b	4.17	0.06	15.0	62.8	0.00	17.84	99.8	37.2	1.2	0.0	1.07	1.44	1.54	6.51	12.02	–	–
Fe-97/3B-gr6-ld..... m	9b	5.47	0.00	18.6	58.6	0.00	17.75	100.4	47.8	1.1	–0.1	1.04	1.87	1.95	6.09	12.03	–	–
Fe-97/3P22a-lh..... m	9c	4.45	0.00	15.1	62.3	0.00	17.77	99.6	38.6	0.7	0.1	1.04	1.52	1.58	6.45	12.00	–	–
Fe-97/3P22a-lm..... m	9c	4.77	0.00	16.3	60.9	0.00	17.77	99.8	41.7	1.0	–0.2	1.05	1.63	1.71	6.33	12.04	–	–
Fe-97/3P22a-ld..... m	9c	5.53	0.00	18.6	57.5	0.00	17.49	99.2	48.7	0.8	0.2	1.03	1.92	1.98	6.05	11.99	–	–
Fe-97/3a-grx-lm..... m	9d	4.46	0.00	15.1	62.7	0.00	17.92	100.2	38.5	0.7	–0.2	1.04	1.51	1.57	6.46	12.04	–	–
Fe-97/3a-grx-ld1..... m	9d	4.90	0.00	16.1	61.1	0.00	17.83	100.0	41.9	0.2	–0.2	1.01	1.67	1.68	6.32	12.02	–	–
Fe-97/3a-grx-ld1'.... m	9d	4.72	0.00	15.4	62.0	0.00	17.85	99.9	40.0	0.1	–0.1	1.00	1.60	1.60	6.40	12.01	–	–
Fe-97/3a-grx-ld2..... m	9d	5.41	0.00	18.3	58.7	0.00	17.58	100.0	47.2	0.9	0.7	1.04	1.85	1.92	6.11	11.93	–	–
Fe-97/3B-gr35-lh..... m	9e	4.22	0.06	15.1	63.0	0.00	18.02	100.3	37.4	1.1	–0.5	1.06	1.45	1.54	6.50	12.08	–	–
Fe-97/3B-gr35-lm.... m	9e	4.71	0.06	16.5	61.7	0.00	17.94	100.9	41.2	0.9	0.2	1.05	1.61	1.68	6.35	12.00	–	–
Fe-97/3B-gr35-ld1.. m	9e	5.47	0.00	18.6	58.6	0.00	17.75	100.4	47.7	1.1	–0.1	1.04	1.87	1.95	6.09	12.03	–	–
Fe-97/3B-gr35-ld2.. m	9e	5.49	0.00	18.7	58.6	0.00	17.79	100.6	47.9	1.0	–0.2	1.04	1.87	1.96	6.08	12.04	–	–
Fe-97/3B-gr22-mtrh. m	9f	4.21	0.07	15.0	63.2	0.00	17.67	100.2	37.2	1.0	1.7	1.05	1.45	1.53	6.51	11.81	–	–
Fe-97/3B-gr22-mtrh'. m	9f	4.33	0.08	15.6	63.0	0.00	17.65	100.6	38.3	1.2	2.2	1.06	1.48	1.58	6.47	11.76	–	–
Fe-97/3B-gr22-lm2.. m	9f	4.56	0.05	15.8	62.1	0.00	17.53	100.1	39.8	0.8	2.2	1.04	1.56	1.62	6.41	11.76	–	–
Fe-97/3B-gr22-lm1.. m	9f	4.80	0.02	16.6	60.6	0.00	17.96	99.9	42.3	1.0	–1.3	1.05	1.65	1.73	6.31	12.18	–	–
Fe-97/3B-gr22-ld.... m	9f	5.50	0.00	18.8	57.7	0.00	17.78	99.8	48.6	1.1	–1.1	1.05	1.90	1.99	6.06	12.16	–	–
Fe-97/3a-grz-lh..... m	10	4.05	0.13	15.0	62.8	0.00	17.93	99.9	36.7	1.1	–0.3	1.06	1.42	1.51	6.53	12.06	–	–
Fe-97/3a-grz-lm..... m	10	4.37	0.11	15.8	61.8	0.00	17.78	99.9	39.2	1.0	0.4	1.05	1.53	1.60	6.43	11.97	–	–
Fe-97/3a-grz-ld1..... m	10	4.60	0.09	16.3	60.8	0.00	17.72	99.4	41.0	0.8	0.0	1.04	1.61	1.67	6.36	12.02	–	–
Fe-97/3a-grz-ldd..... m	10	5.35	0.06	18.4	57.9	0.00	17.53	99.2	47.5	0.7	0.1	1.03	1.87	1.93	6.10	12.00	–	–
Fe-99/72-gr21-m..... m	13a	0.40	0.00	1.5	79.5	0.08	18.61	100.0	3.4	0.2	0.2	1.12	0.13	0.14	7.86	11.98	–	–
Fe-99/72-gr21-d..... m	13a	4.00	0.00	13.7	65.1	0.00	17.92	100.6	34.3	0.8	1.0	1.05	1.34	1.40	6.63	11.90	–	–
Fe-99/68-gr1-m..... m	13b	0.57	0.00	2.2	78.4	0.09	18.61	99.9	5.1	0.5	–0.3	1.20	0.19	0.22	7.80	12.04	–	–
Fe-99/68-gr1-d..... m	13b	4.05	0.05	14.0	64.1	0.11	18.11	100.4	35.1	0.5	–0.5	1.03	1.38	1.42	6.60	12.08	–	–

Notes: The compositions are expressed in terms of weight % constituents, then recast as empitrical formulae. Estimated standard deviations for the analytical results are as follows: Cu (0.05), Fe (0.01), Pb (0.25), Bi (0.35), Sb (0.05) and S (0.07). Definitions of n_{atk}, Δn_{atk}, ev, and the empirical formulae are explained in Table 1. area% and BD represents relative area of phases present in the image and initial composition of exsolved grain in terms of n_{atk}, respectively.

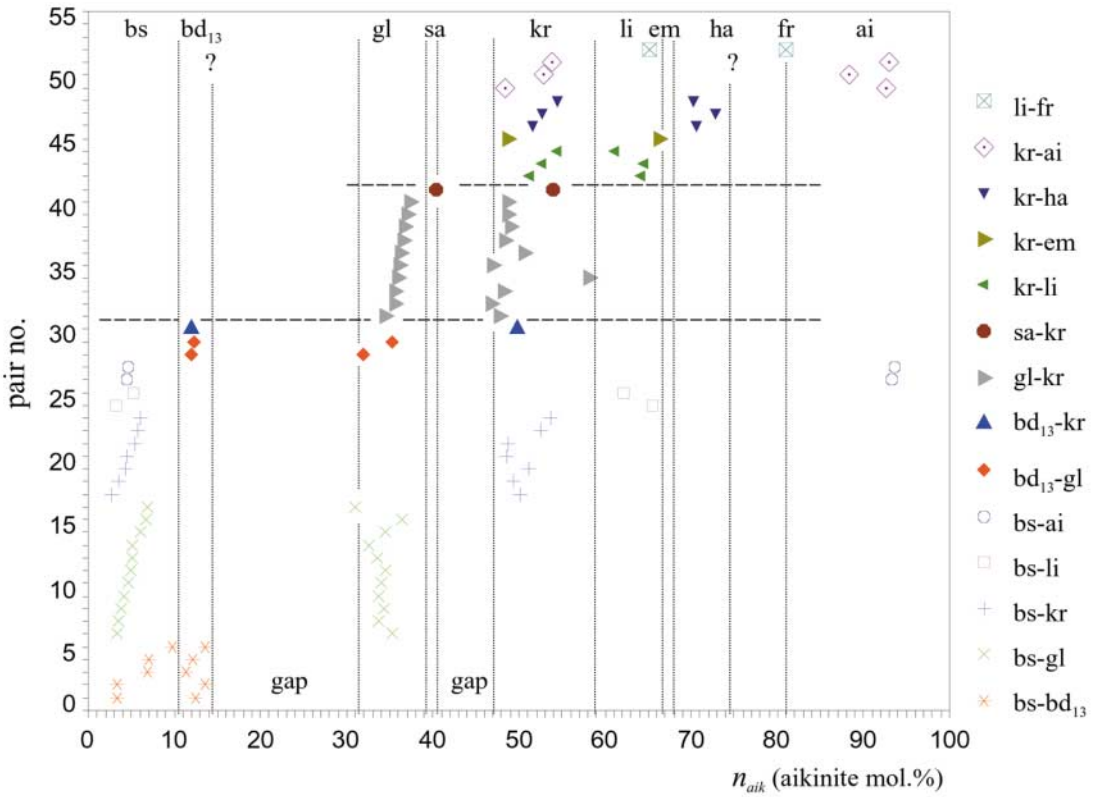

FIG. 4. Pairs of coexisting homogeneous bismuthinite derivatives typifying the disequilibrium and replacement associations from Felbertal. For abreviations, see Figure 2. Boundaries between the fields assigned to distinct derivatives are of orientational value only; for exact data, see Table 1.

Perusal of a large number of observed cases [Tables 2 and 4 (deposited), and Fig. 4] allows definition of three replacement trends in the Felbertal deposit: 1) those with the end-product being krupkaite, the starting material varying from n_{aik} = 93 to n_{aik} = 62, 2) those with the end-product being gladite, starting generally from stoichiometric to oversubstituted krupkaite (Cu- and Pb-bearing krupkaite), and 3) those with the end-product being bismuthinite, rarely also bd_{13}. In this case, the starting derivatives span practically the entire range of bismuthinite–aikinite series, from aikinite to bd_{13}.

Other replacement pairs are rare, *e.g.*, the association $bd_{54} \rightarrow bd_{40.4}$ in Figure 3b. In several instances, two-step replacement is observed, *e.g.*, $bd_{50} \rightarrow bd_{37} \rightarrow bd_5$ (Fig. 3e). In this and other one-step instances, the compact late bismuthinite derivative with n_{aik} in the bismuthinite range is in some cases associated with chalcopyrite–bismuthinite symplectite, which roughly replace decomposed grains of, presumably, an original Cu–(?)Fe–Bi sulfosalt.

EXSOLUTION PAIRS

Exsolution pairs that formed from original single bd grains represent the majority of bd aggregates at Felbertal. Elongate drops to wavy lamellae of one component are quasi-regularly distributed in the matrix of the major phase (Fig. 5), in some cases showing a predilection for the ancient planes of weakness. With few exceptions, the BSE images show that both exsolved phases are chemically homogeneous.

Careful analyses of exsolution products by means of the electron microprobe gave the first indication of the chemical complexity of the exsolved phases and the existence of new, hitherto undescribed phases. Well-organized exsolution lamellae in which the two exsolved phases differ by δn_{aik} of 2–3% were later found to correspond fully to two crystallographically distinct although chemically very similar phases (Table 1).

The best developed and most common examples are the exsolved phases in the gladite–krupkaite range

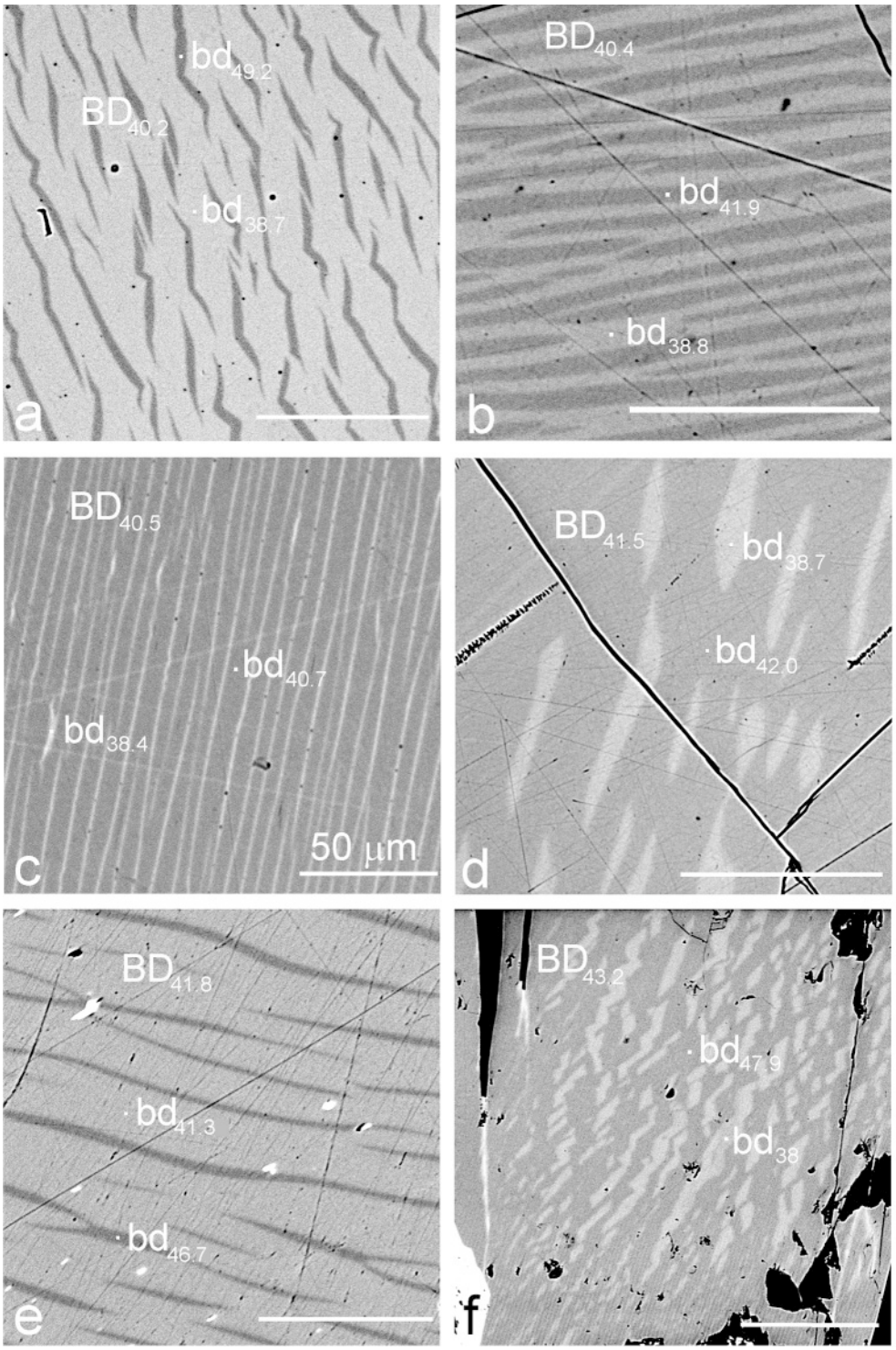

FIG. 5. Exsolution pairs in the bismuthinite–aikinite derivatives (the gladite–krupkaite range) from the Felbertal deposit. Distinct associations are illustrated, originating from bulk compositions (capital letters) clustered around n_{aik} intervals of 40.2–40.5,

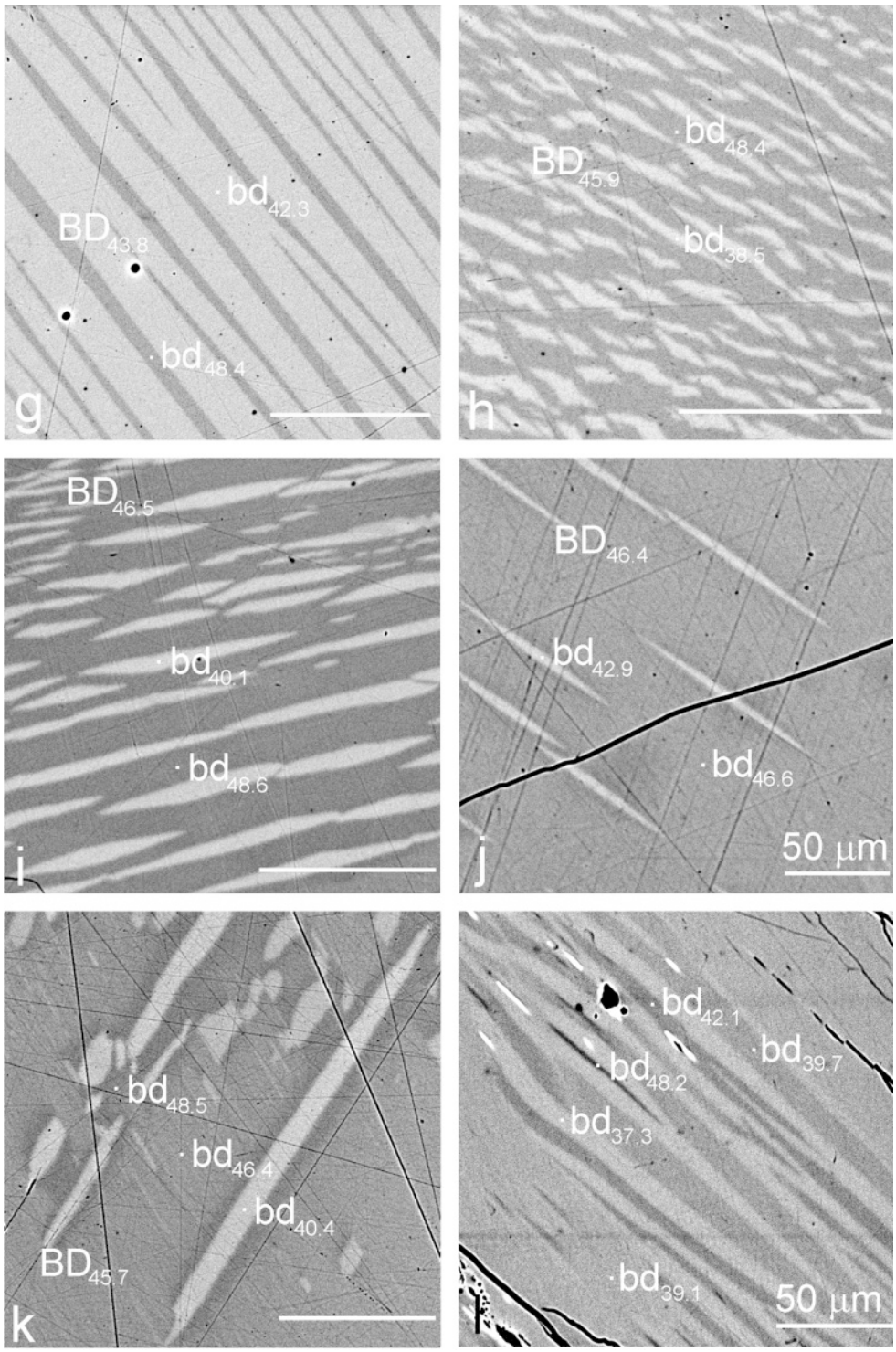

41.5–41.8, 43.2–43.8, and 45.9–46.5. Where not indicated, bar length is 100 μm. Figure 5*l* shows a sequence of pairs, $bd_{37.3}$ – $bd_{39.7}$, $bd_{37.3}$ – $bd_{42.1}$, and, finally, $bd_{37.3}$–$bd_{48.2}$ developed from the original composition $bd_{39.1}$.

[Table 2 and 5 (deposited), Figs. 5, 6], for which the exsolved phases can be identified as classical or new mineral species. A combination of electron-microprobe data on exsolved species with image analysis allowed us to estimate the original, pre-exsolution composition of the bd phase (given as BD below). Table 2 and Figure 6 show that the krupkaite ($bd_{48.5}$) – paarite ($bd_{42.5}$) aggregate formed from $BD_{46–47}$, the krupkaite ($bd_{48.5}$) – salzburgite ($bd_{40.5}$) aggregate, from $BD_{45–47}$, and the krupkaite ($bd_{48.5}$) – gladite ($bd_{38.5}$) aggregate, from $BD_{45–46}$ (Table 2, Fig. 6), *i.e.*, all three cases have roughly the same starting composition. The exsolution of the original $BD_{\sim 46}$ phase situated in the paarite–krupkaite gap into the association of krupkaite (in which we observe gradual enrichment in Cu–Pb, indicated by different shades of grey in Figs. 5j, k), with $bd_{42.9}$, $bd_{40.1–40.4}$, and $bd_{38.5}$, respectively, is illustrated in Figures 5h–k.

Pre-exsolution compositions with lower n_{aik} values abound as well: the pair gladite (bd_{37}) – krupkaite ($bd_{48.5}$) exsolved from $BD_{38.5}$, the same pair containing more Cu-rich gladite ($bd_{\leq 38.7}$) exsolved from BD_{40} and BD_{43}, respectively. The pair gladite (bd_{37}) – salzburgite (bd_{41}) formed from BD_{40}, whereas high-Cu gladite ($bd_{38.5}$) – paarite ($bd_{42–43}$) formed from a range of salzburgite-like compositions. The principal exsolution-related pairs plotted in Figure 6 are illustrated in Figures 5a–c, d–e, f–g for the starting bulk-compositions clustered on $BD_{40.2–40.5}$, $BD_{41.5–41.8}$, and $BD_{43.2–43.8}$, respectively. The compositions shown in Figure 6 were ordered according to the composition of the phase poorer in Cu–Pb in order to establish possible related compositional trends in the high-Cu phases; however, only weak and partly contradictory trends were found. Chemical compositions of very fine lamellae were not included. A crystallographic confirmation of exsolution trends was found in the single-crystal X-ray-diffraction study of a grain of $bd_{42.6}$ in which the original 5-fold superstructure decomposed partly into a mixture of 3-fold and, presumably, 1-fold structure (Table 1).

Exsolution pairs in the bismuthinite–gladite region [Tables 2 and 4 (the latter deposited) and Figs. 7, 8] are less common in the Felbertal deposit and not so well documented. Gladite ($bd_{\geq 33}$) is the most common com-

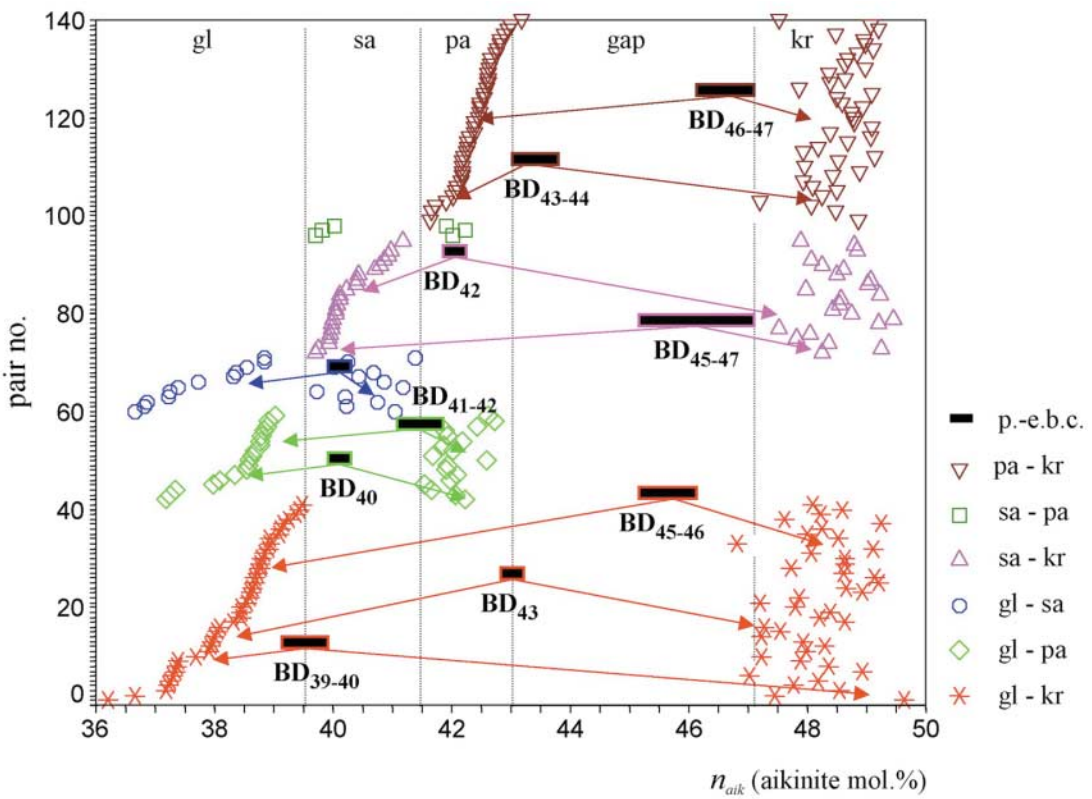

FIG. 6. Exsolution pairs of bismuthinite derivatives in the gladite–krupkaite range with pre-exsolution bulk-compositions (p.-e.b.c.) of selected exsolution-induced aggregates indicated by black bars. Symbols indicate types of association. Boundaries between the fields assigned to distinct derivatives are of orientational value only.

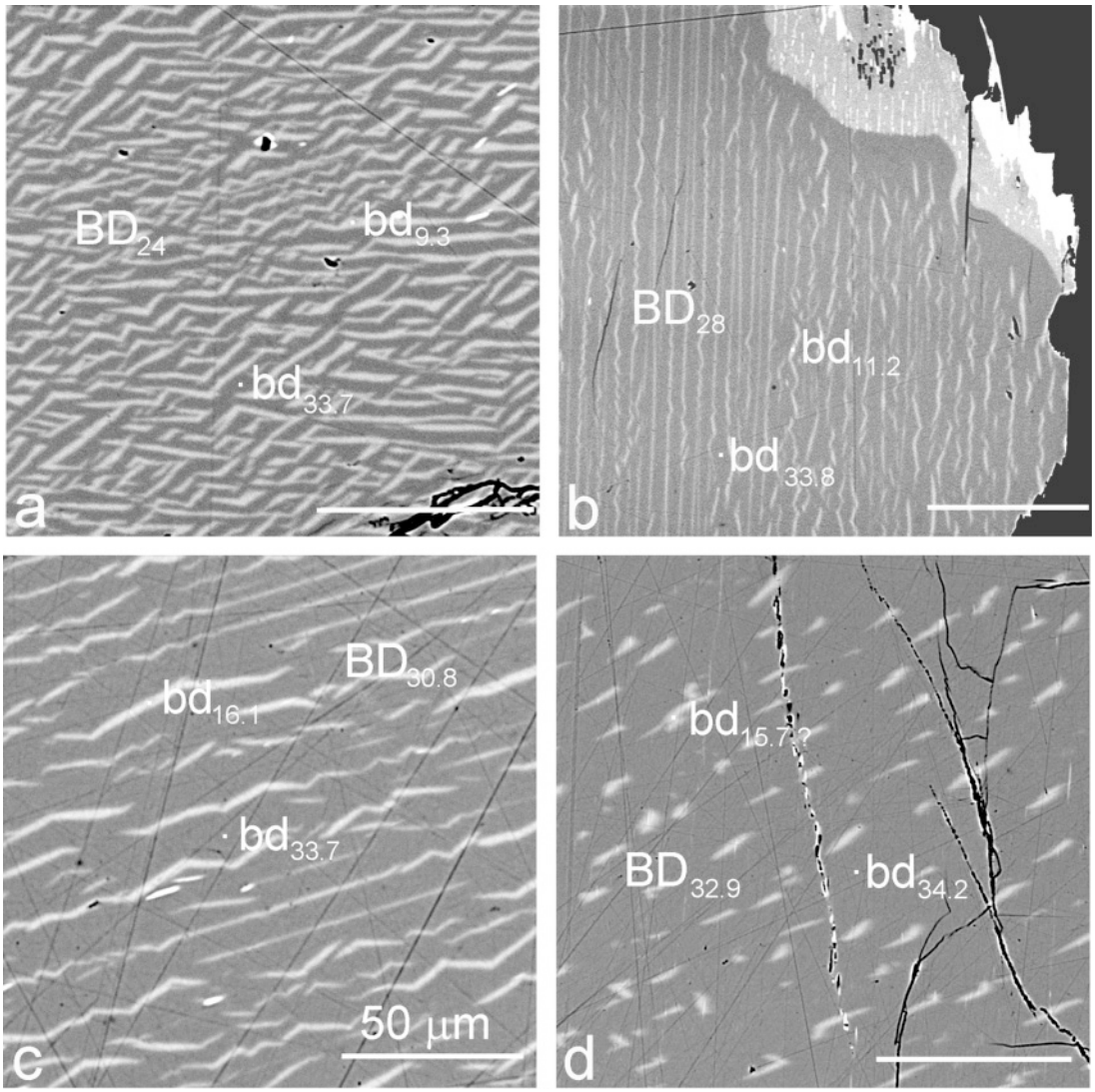

FIG. 7. Exsolution pairs in the bismuthinite–aikinite derivatives (the bismuthinite–gladite range) from the Felbertal deposit. Distinct associations originating from bulk compositions (capital letters) having n_{aik} = 24, 28, 31 and 33, are illustrated.

ponent. It associates with bismuthinite (bd_{10}), pekoite (bd_{16}), but also with the rather frequent lamellae bd_{13}. Less frequent are lamellae $bd_{21–22}$ and $bd_{25–27}$, which associate with bd_{13}, pekoite and, in a single case, with gladite (Fig. 8). None of these bd phases was found as a single, unexsolved grain.

COMPLEX EXSOLUTION AGGREGATES

Some exsolution aggregates contains more than two distinct bismuthinite derivatives, the number of such components increasing up to five. For three-component grains, microscopic observations always indicate lamellar aggregates in which the "third" phase either is developed as residual areas (slabs) of the original bulk-composition or it is a phase exsolved in the earlier stage of exsolution and is clearly being replaced by a new, compositionally more extreme bismuthinite derivative (Figs. 9a–c). The latter type either occurs as the continuation of the older exsolved lamella (Figs. 9a–c) or, less commonly, it coats a lamella of the older phase at its contacts with the other, persisting exsolved com-

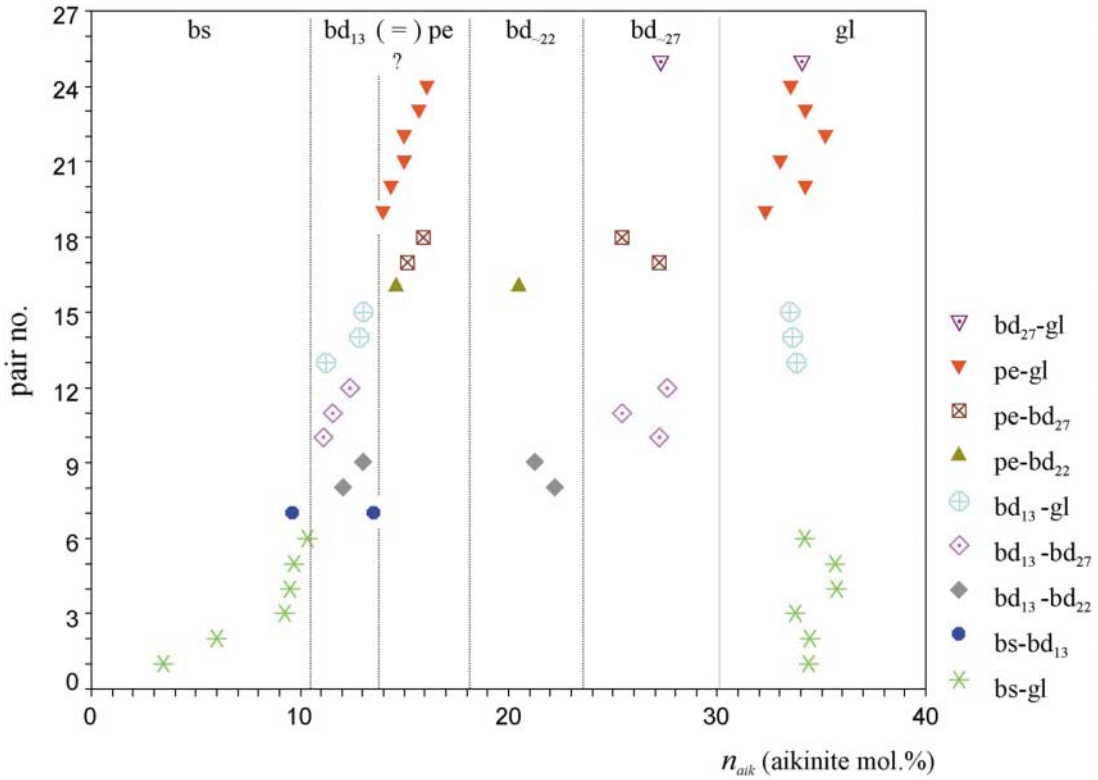

FIG. 8. Exsolution pairs of bismuthinite–aikinite derivatives in the bismuthinite–gladite range. Symbols indicate types of association.

ponent (Figs. 9b, e). This persisting component is common to the early and the late exsolution association; only exceptionally was a slight change in its composition observed (the krupkaite component in Fig. 9e). In cases where the compositional difference increased in the transition from the earlier to the later association, the relative amount (lamella thickness) of the unchanged, persisting exsolved component increases and the lamellae of the newest component are thinner than those of the component being consumed (Figs. 9a, c).

Polished grains in which four distinct bd components were observed combine these two principles: both the areas of original, single composition exist, and an alteration sequence for one of the two primarily exsolved phases is observed. In the most dramatic example (Fig. 10), the original $bd_{39.2}$ phase (Cu–Pb-rich gladite) decomposes into gladite, $bd_{36.7}$, and salzburgite, $bd_{41.1}$. The latter locally alters into krupkaite ($bd_{47.5}$) with a dramatic decrease in lamella thickness and a corresponding increase in the volume of gladite ($bd_{36.7}$).

A sequence of laterally proceeding modifications, $bd_{40.1} \rightarrow bd_{41.9} \rightarrow bd_{47.2}$ (all in association with $bd_{38.5}$) is illustrated in Figure 9d, in which no primary phase is present. Among the rare instances of five-component bd intergrowths, Figure 9f shows a sequence from an exsolution pair that is not quite well defined, $bd_{38.3}$–$bd_{39.8}$, to the final pair $bd_{37.2}$–$bd_{48.6}$. Figure 5*l* presents an exsolution sequence starting with $bd_{39.1}$ that on the one hand produced lamellae of persisting gladite ($bd_{37.3}$) and, on the other, a sequence $bd_{39.7} \rightarrow bd_{42.1} \rightarrow bd_{48.2}$, all within a span of 150 μm.

Estimates of compositions of the precursor in the case of the exsolution pairs from the grains with three to four components are infrequent, owing to the

FIG. 9. Evidence of multistage exsolution for the bismuthinite–aikinite derivatives in the Felbertal deposit. a) Modification of bd_{42} lamellae into bd_{49} lamellae (plus additional bd_{39}) advancing from grain boundary; b) similar process for $bd_{40.2} \rightarrow bd_{47.8}$ on a diagonal plane of weakness and from grain margin ($bd_{47.8}$ overgrowing $bd_{40.2}$, associated with $bd_{37.4}$); c) a virtually completed second stage of exsolution; d) evidence of three-stage exsolution, with exsolved lamellae creating a sequence $bd_{40.1} \rightarrow bd_{41.9} \rightarrow bd_{47.2}$; e) the exsolution pair $bd_{41.2}$–$bd_{47.7}$ being replaced by $bd_{37.4}$–$bd_{47.9}$; f) lobed remnants of $bd_{\sim 39}$ with indistinct lamellae of $bd_{39.8}$ being replaced by the matrix $bd_{37.2}$ and a sequence of exsolution lamellae $bd_{39.8} \rightarrow bd_{42.3} \rightarrow bd_{48.6}$.

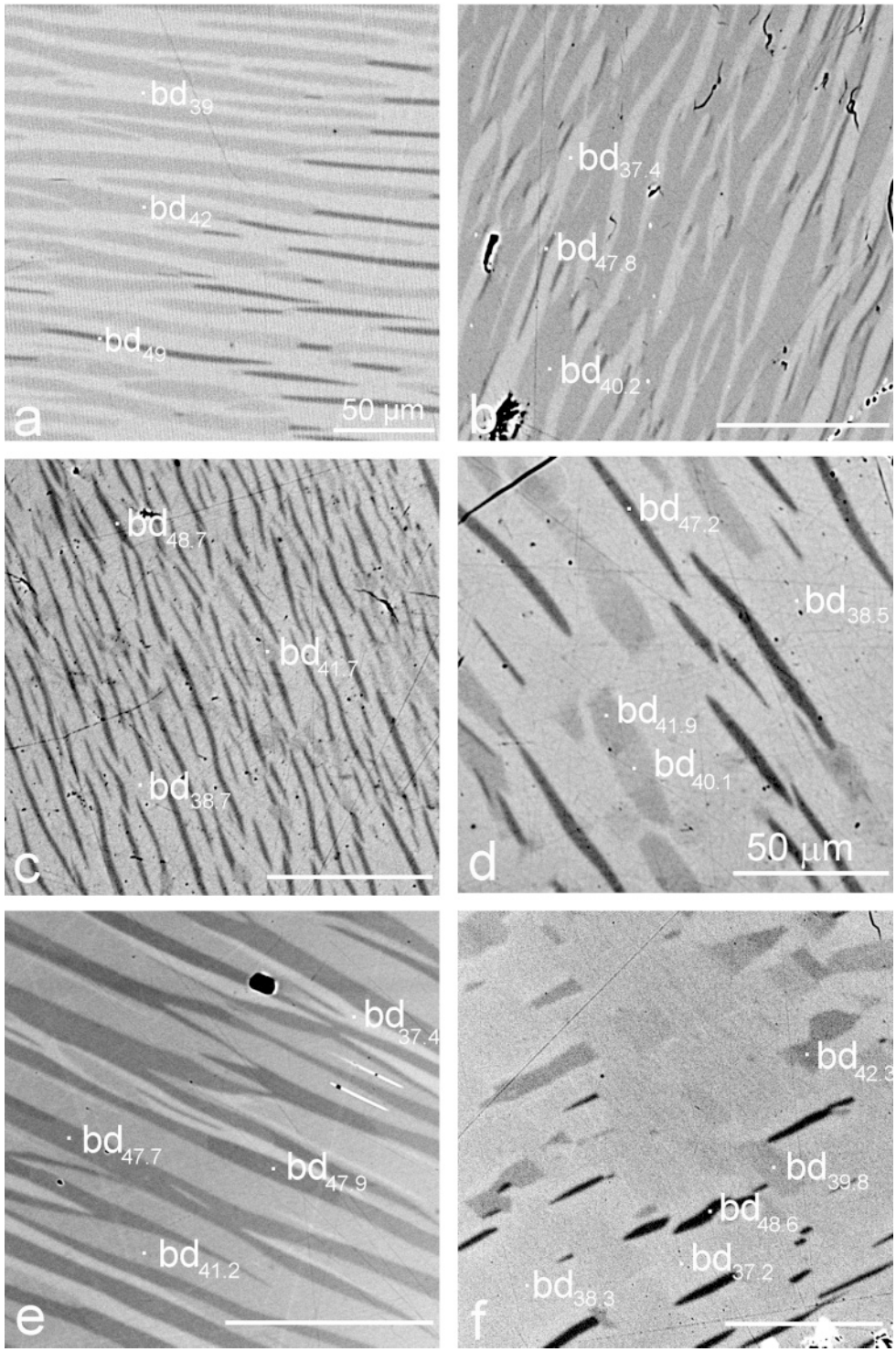
bd39
bd42
bd49
50 µm
a
bd37.4
bd47.8
bd40.2
b
bd48.7
bd41.7
bd38.7
c
bd47.2
bd38.5
bd41.9
bd40.1
50 µm
d
bd37.4
bd47.7
bd47.9
bd41.2
e
bd42.3
bd39.8
bd48.6
bd37.2
bd38.3
f

difficulty in separating sufficiently large, representative areas for each of the pairs present in the process of image analysis. Image analysis of a well-developed exsolution-induced intergrowth with a large original core of $BD_{40.3}$ and two areas of lamellar intergrowths (the first-stage association $bd_{38.8} - bd_{41.9}$ and the subsequent association $bd_{38.8} - bd_{48.0}$) gave BD_{40} as a bulk composition for both associations.

Discussion and Conclusions

The results of our studies complicate substantially the solvus of the pseudobinary system $Bi_2S_3 - CuPbBiS_3$ in the gladite–krupkaite region. Suggestions for similar complications were also found in the bismuthinite–gladite region, whereas no exsolution textures were located for the derivatives with n_{aik} over 50. Our initial simple working model for the gladite–krupkaite region was based on the assumption of a stable final association gladite–krupkaite. The first (*i.e.*, highest-temperature) association would be paarite–krupkaite as the first precursor, invariably followed by the association salzburgite–krupkaite at a somewhat lower temperature, which would finally yield the stable pair gladite (bd_{33}) – krupkaite (bd_{50}). This model implies that salzburgite invariably decomposes into gladite and krupkaite, and that sequences of consecutive exsolution-lamellae such as $bd_{39.7} \rightarrow bd_{42.1} \rightarrow bd_{48.2}$ from the original bd_{39}, occurring in every case in association with $bd_{37.3}$ lamellae (Fig.5*l*), are impossible.

None of these assumptions was fulfilled, however; the $bd_{\sim 38–40}$ compositions yield equally well two-phase intergrowths with the "allowed" or the "forbidden" combinations of phases (Fig. 5), even the salzburgite–paarite exsolution aggregates were observed, and the above "forbidden" temporal sequence of lamellae, salzburgite → paarite → krupkaite in association with gladite, is common (Figs. 5*l*, 9d and f). The other possibility, paarite being stable to lower temperatures than salzburgite, would preclude the associations of the type observed in Figure 5i, in which the original $BD_{46.5}$ exsolves into krupkaite, $bd_{48.6}$, and salzburgite, $bd_{40.1}$. Therefore, an alternative explanation was sought which would explain all the observed facts.

Being structural combinations (*i.e.*, mixtures) of just two types of tightly bonded ribbons (or of two types of structure modules), the individual derivatives of bismuthinite in the gladite–krupkaite range do not differ substantially in their Gibbs free energy. Because of this, the activation energy of ordering assumes a dominant role in the exsolution process, in which not only the easy redistribution of copper atoms and vacancies but also the much more difficult redistribution of lead and bismuth atoms take place. Therefore, the disordered or ordered parent phase exsolves into two compositionally adjacent ordered derivatives, involving a minimum of diffusion and compositional separation, and not into a more widely separated pair, which might be thermodynamically more stable. In all observed cases, further development toward more stable, and more distinct, separate compositions proceeds *via* an analogous pro-

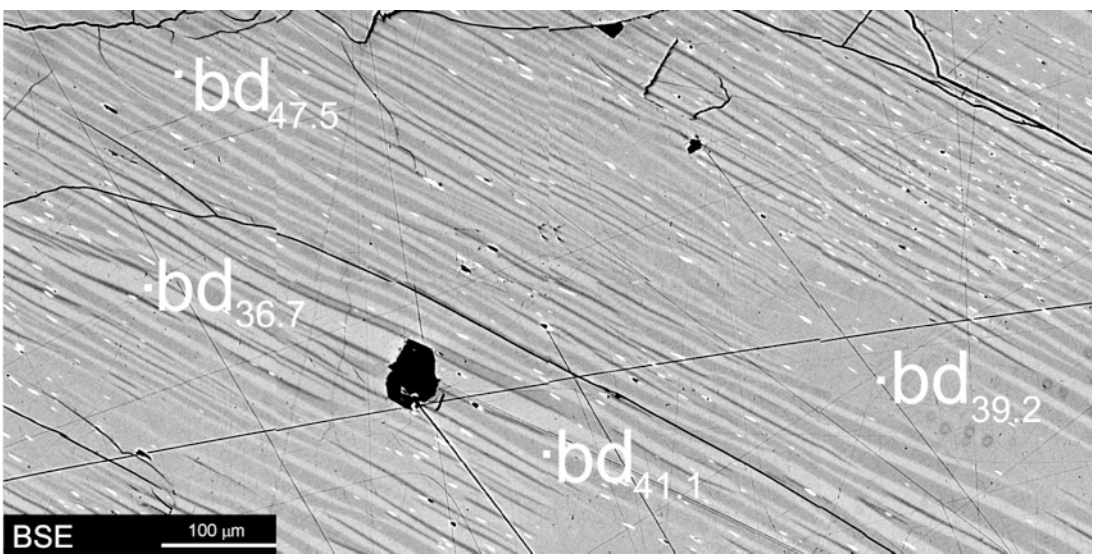

FIG. 10. Large-scale development of exsolution patterns in a crystal of $bd_{39.2}$ from Felbertal. Flat-grey area: original phase; light and medium grey lamellae: $bd_{36.7}$–$bd_{41.1}$ intergrowth. Light and dark lamellae: second-stage exsolution producing krupkaite–gladite intergrowth in selected zones.

cess in one (presumably metastable) member of the pair, again yielding a pair of structures compositionally closest to the decomposing derivative. This process again involves minimal changes in the previous pattern of Cu and Pb–Bi distribution. The difficult ordering process might be facilitated by a local development of structural faults or, more probably, by the influence of intergranular fluids as suppliers of itinerant protons able to catalyze local interchange of cations by temporarily attaching themselves to the sulfur atoms involved. Both of these factors would cause the zonal and patchy development of the younger exsolution-induced associations, observed in our material.

The highest portion of the solvus for the two observed compositional gaps in Figure 2 might well reach into the disordered regions of the bismuthinite–aikinite solid solution, but the fine aggregates of exsolution products just described, with small compositional differences between the exsolved components, and with the observed sequential development, are connected with the existence of ordered, compositionally clearly defined phases.

Owing to its predominantly kinetic nature, the exsolution process in the gladite–krupkaite range of the bismuthinite–aikinite series does not allow us to recognize and define the thermodynamically determined shape of the solvus and the relative stability of individual derivatives, with the exception of the apparently most stable, terminal gladite–krupkaite association. Our studies show that factors related to thermodynamic stability are overshadowed by the kinetic ones in the ordering processes in Nature.

The exsolution aggregates in the bismuthinite–gladite region resemble texturally those from the gladite–krupkaite interval, in sharp contrast to the aggregates with n_{aik} over 50. In the latter, no clear exsolution textures were recognized, even where the X-ray data confirmed a mixture of two derivatives (*e.g.*, lindströmite and oversubstituted krupkaite). A possible explanation is contained in Figure 11, in which data from Table 1 were used. The linear change in the subcell volume throughout the series is accompanied by a similarly linear change in the length of the 4 Å parameter (*a* dimension) but by an opposite, two-step change in the

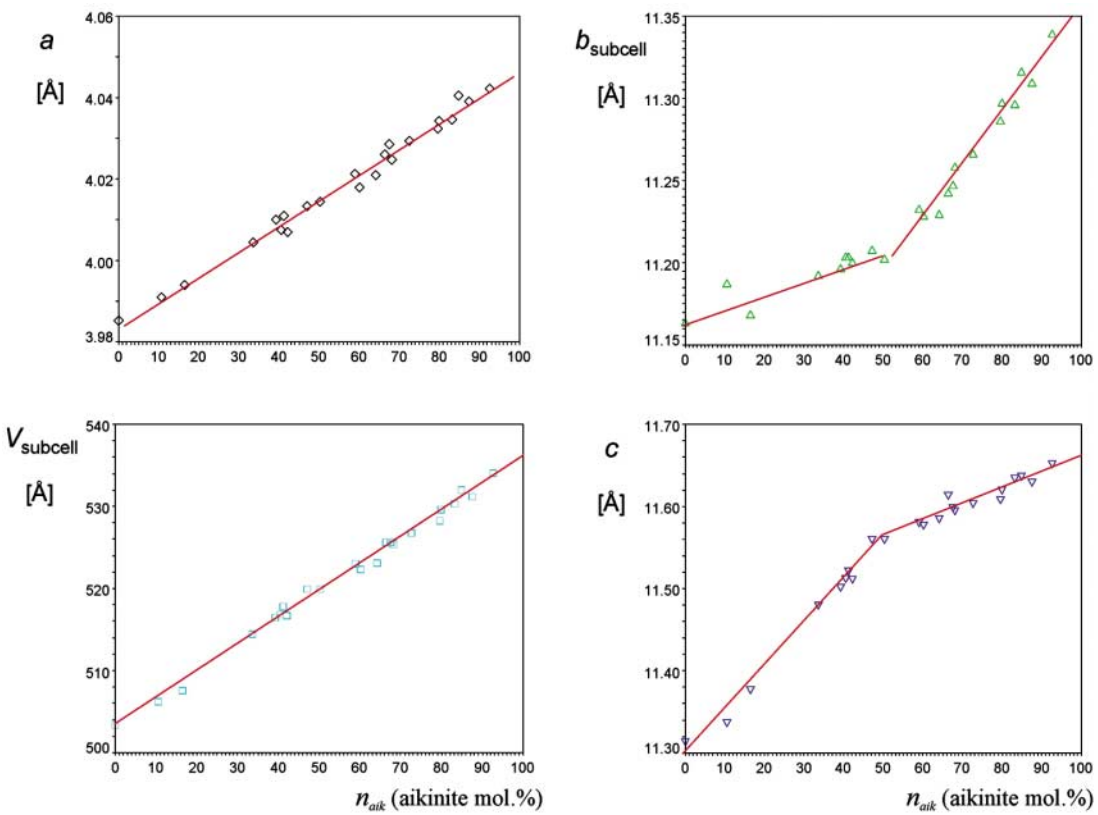

FIG. 11. Change in subcell dimensions with increasing molar percentage of the aikinite component.

b and *c* parameters (Fig. 11). In the case of two coexisting phases, excessive strain or incoherency will develop along contact planes containing the lattice vector with the steep trend in Figure 11.

Although the ordering process proceeds by building (010) modules of various types, the exsolution lamellae of two phases in the bismuthinite–aikinite series should form most easily on the planes of least elastic strain. Thus, the two trends in the development of *b* and *c* parameters, below and above $n_{aik} = 50$, should have a profound influence on the exsolution forms and kinetics. They might cause the submicroscopic character of nearly all observed exsolution-lamellae in the krupkaite–aikinite range (*i.e.*, $n_{aik} > 50$) range. Final confirmation of these ideas can only be obtained by a combination of microscopic and diffraction studies on the exsolution intergrowths in this range.

The temperatures of exsolution and ordering are unknown. The synthetic materials produced by Springer (1971) at 300°C and by Mumme & Watts (1976) at 500°C are disordered, with an 11Å cell only, and no recognized superstructure (the latter authors also used single-crystal X-ray diffraction). Pring (1995) observed cation ordering and superstructure formation in synthetic $Cu_2Pb_2Bi_4S_9$ (hammarite) at 175° and 225°C after extended annealing. First, after 32 months at 175°C, a non-periodic sequence of krupkaite and aikinite strips (010) of finite length appeared. It is replaced by fairly regular 3*a* sequences (with occasional 4*a* intervals) after the total of 56 months at 225°C. Development of strip sequences was very unequal in different fragments of the same charge.

The applicability of these observations to the principal body of our data is somewhat limited; they concern the compositions above 50 mol.% of the aikinite component, not available in our exsolution aggregates. Thus we can only tentatively accept the above temperatures for our conditions. The catalysis of diffusion processes by the influence of tectonics and fluids, suggested here, still awaits experimental verification.

Very good insight into the shape and orientation of exsolution lamellae in the $n_{aik} < 50$ range was obtained from a combination of BSE images of the exsolution textures with the observed (001) cleavage of low-Cu bismuthinite derivatives. In the sections of crystals approximately parallel to (100), the exsolution takes the form of straight lamellae → wavy lamellae → shorter or longer zig-zag lamellae → skeletal rhomb-like arrangements of lamellae → rhomb-shaped rods and their strings (Figs. 5, 7). In the best-oriented sections, the angle comprised by the lamellae (or surfaces of rhomb-like rods) varies between about 110° and 135°. Its complement, 70°–45°, is bisected by the (001) cleavage planes.

Examination of the crystal structures of bismuthinite derivatives reveals that for the range bd_0–bd_{50}, in which the smallest increments (*i.e.*, differences) occur on the *b* axis, the planes of minimum elastic strain will be those filled by lone pairs of electrons of the Bi and Pb atoms and the long cation–sulfur interactions. These are (a) the slightly wavy (100) planes, (b) planes $(012)_{subcell}$ with occasional, periodic cross-chains protruding slightly from the smooth surface, (c) planes $(011)_{subcell}$ with a stepped surface, and (d) planes $(013)_{subcell}$, which combine properties of both previous planes.

The (012) planes comprise an angle of ~126°, the (011) planes, of ~90°, whereas the (013) planes show an angle of ~140°, depending on the derivative. The most exact values observed in polished sections fit best the exsolution on $(012)_{subcell}$ planes, although the local twists and turns of the lamellae (Figs. 5, 7) suggest that they might follow alternatively any of these three low-strain planes. Very locally, clear cases of (011) planes appear, as in Figure 7.

The spatial distribution of bismuthinite–aikinite derivatives and of their replacement and exsolution pairs in the deposit gives qualitative clues about the conditions of formation and development of the individual orebodies K1–K8. The sampling of the orebody is a function of its accessibility in the past ~15 years. Nevertheless, the overall picture is rather consistent and suggests certain general trends.

There are two pronounced compositional gaps that, with few exceptions, persist throughout the deposit, indicating that the temperatures of formation only rarely were high enough for their potential closure. The first gap, between $bd_{\sim 16}$ and $bd_{\sim 32}$ (pekoite–gladite) is fairly stable; it gets narrower or contains intermediate exsolved phases only in the bodies K1, K3, eventually also K6 and K8 (Fig. 12). The second gap, at its broadest between bd_{37} and bd_{50} (gladite–krupkaite), narrows to bd_{38}–bd_{47} in K8 and K1 and, to a lesser degree, in K7, whereas it is constricted to a narrow gap $bd_{\sim 44}$–$bd_{\sim 47}$ or completely bridged by the pre-exsolution compositions on levels 4–6 of the K3 orebody. So far, the fourth level of the K3 orebody is the only locality for the homogeneous salzburgite and paarite crystals. A similar bridging is largely absent for the previous gap on these levels, although both gaps are outlined by exsolved compositions (Fig. 12).

Summarizing these observations, the K3 orebody apparently formed at the highest temperatures, at which point the bd_{38}–bd_{50} region formed; the same can be assumed for the bd_{16}–bd_{33} region in the K1 body. The associations of the replacement type, with two to three bd phases coexisting, appear most commonly in the smaller orebodies K6–K8 (Fig. 12) . The composition of the phases involved, together with the near-absence of exsolution textures in the bodies K7 and K8, suggest that ore formation was taking place at temperatures at which both large miscibility-gaps were already well delineated, although still narrow in the case of the K8 body.

The interesting question whether the sulfide ore material was molten at the peak temperatures of metamorphism can on the one hand be addressed by review-

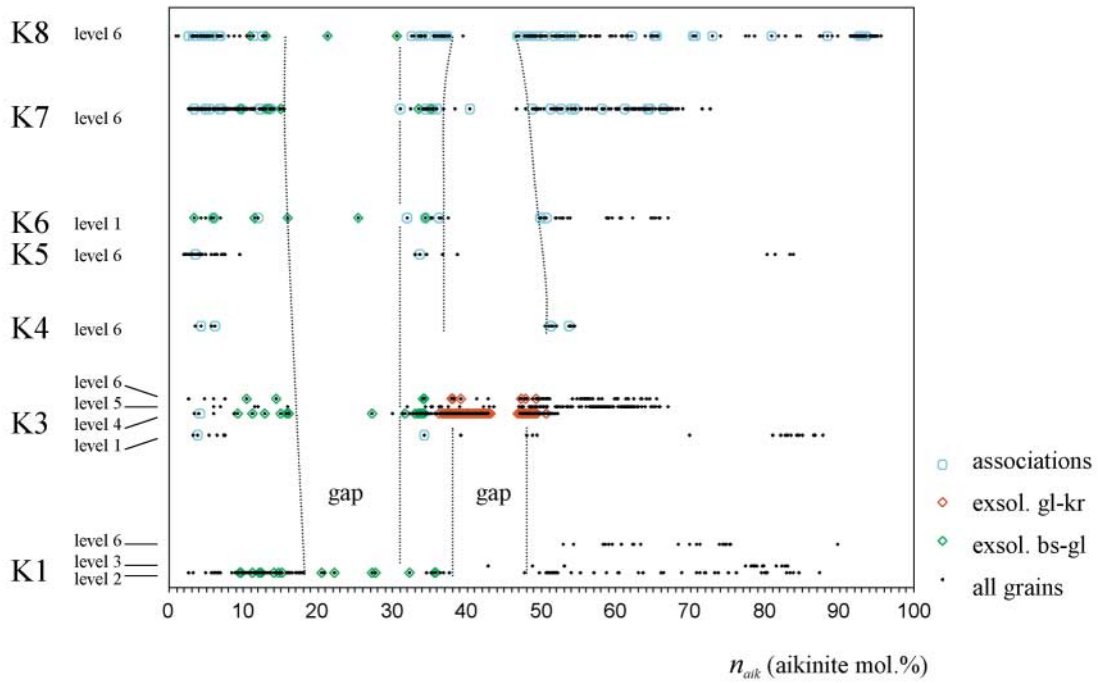

FIG. 12. Electron-microprobe data on bismuthinite–aikinite derivatives in the deposit of Felbertal, distributed over individual studied levels of K1–K8 orebodies. Individual compositions, coexisting compositions, and exsolution grains are distinguished. The observed miscibility-gaps for distinct orebodies are schematically indicated.

ing the known sulfide phase systems and on the other by textural studies. According to Springer (1971), only the aikinite–lindströmite region of the bismuthinite–aikinite solid solution should be molten in the range 550–600°C. No melt was observed in the system PbS–Bi_2S_3–Sb_2S_3 (Chang *et al.* 1980) and Ag_2S–PbS–Bi_2S_3 (Hoda & Chang 1975) at 500°C. The binary eutectic wittichenite–$Cu_3Bi_5S_9$ occurs at about 515°C (Buhlmann 1971, Sugaki *et al.* 1974), and incongruent melting of "$CuBi_3S_5$", *i.e.*, synthetic makovickyite, occurs at 649°C. There is no liquid in the system PbS–Cu_2S–Bi_2S_3 at 400°C (Hoda & Chang 1975) or 450°C (Bente 1980), or in the system Ag_2S–Cu_2S–Bi_2S_3 at 454°C (Chen & Chang 1974) or 500°C (Chang *et al.* 1988). Liquid was observed in the Cu_2S–wittichenite region, at up to 30 mol.% PbS in the system Cu_2S–PbS–Bi_2S_3 at 500°C (Chang *et al.* 1988), and at up to 40 mol.% PbS if Ag_2S is added to the system. Antimony lowers the melting temperature substantially. These observations suggest that the peak-metamorphic melting of the sulfosalt component ought to be restricted to the ore portions richest in copper. The textural observations indicate that any possible textures from this stage were obliterated by later segregation of mineral phases and growth of crystals in the long-duration retrograde stage, and by the competing growth of sulfide and quartz crystals along the ore-inclusion boundaries at this stage of formation.

Processes of reduction, in which bismuthinite–aikinite derivatives, together with other sulfosalts, are reduced to native bismuth plus other products of decomposition, are late and have no connection to the extensive replacement processes in which one sulfosalt (assemblage) replaces another (Fig. 13b).

ACKNOWLEDGEMENTS

This research was supported by a grant to D.T. from the University of Salzburg, Austria and by project No. 9901772 of the Danish Natural Science Council. The diffraction equipment used was financed by the Danish Natural Science Research Council. Support from both institutions and the University of Copenhagen is gratefully acknowledged. The kind interest of Dr. Peter Walser, Superintendent of the Wolfram Bergbau GmbH Nachfolger CG, and logistical assistance of Mr. H.J. Zoller, are greatly appreciated. We thank Dr. Allan Pring, an anonymous reviewer, and Robert F. Martin for their critical comments, which helped to improve the paper.

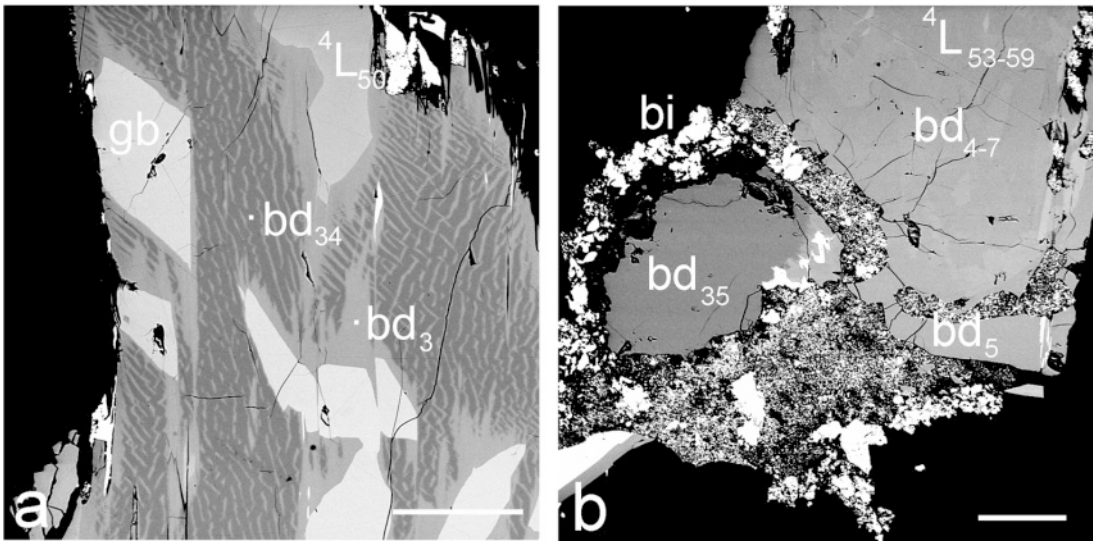

FIG. 13. a) A subparallel aggregate of (presumably) gladite, replaced from margins by Cu-bearing bismuthinite. The transition zone developed in the grain cores subsequently exsolved into a bd_{34}–bd_3 intergrowth. Associated phases: galenobismutite (gb) and lillianite ($^4L_{50}$). b) A grain of gladite (n_{aik} = 35) partly replaced by bd_5, as well as a large complicated intergrowth of $bd_{5–7}$ with lillianite ($^4L_{53–59}$); both are corroded and replaced by a mixture of native bismuth (bi) with fine-grained secondary products.

REFERENCES

BALIĆ-ŽUNIĆ, T., TOPA, D. & MAKOVICKY, E. (2002): The crystal structure of emilite, $Cu_{10.7}Pb_{10.7}Bi_{21.3}S_{48}$, the second 45 Å derivative of the bismuthinite–aikinite solid-solution series. *Can. Mineral.* **40**, 238-245.

BENTE, K. (1980): Experimentelle Untersuchungen an Cu–Pb–Bi-Sulfosalzen im Sytem CuS–Cu_2S–PbS–Bi_2S_3. *Neues Jahrb. Mineral., Monatsh.*, 385-395.

BRIEGLEB, D. (1991): Die Scheelitlagerstätte im Felbertal bei Mittersill. *Ber. Deutsch. Mineral. Geselsch.* **2**, 48-50.

BRUKER AXS (1997): SHELXTL, Version 5.1. Bruker AXS, Inc., Madison,Wisconsin 53719,U.S.A.

_____ (1998): SMART, Version 5.0. Bruker AXS, Inc., Madison,Wisconsin 53719,U.S.A.

_____ (1998): SAINT, Version 5.0. Bruker AXS, Inc., Madison,Wisconsin 53719,U.S.A.

BUHLMANN, E. (1971): Untersuchungen im System Bi_2S_3–Cu_2S und geologische Schlussfolgerungen. *Neues Jahrb. Mineral., Monatsh.*, 137-141.

CHANG, L.L.Y., WALIA, D.S. & KNOWLES, C.R. (1980): Phase relations in the system PbS–Sb_2S_3–Bi_2S_3 and PbS–FeS–Sb_2S_3–Bi_2S_3. *Econ. Geol.* **75**, 317-328.

_____, WU, DAQING & KNOWLES, C.R. (1988): Phase relations in the system Ag_2S–Cu_2S–PbS–Bi_2S_3. *Econ. Geol.* **83**, 405-418.

CHEN, T.T. & CHANG, L.L.Y. (1974): Investigation in the system Ag_2S–Cu_2S–Bi_2S_3 and Ag_2S–Cu_2S–Sb_2S_3. *Can. Mineral.* **12**, 404-410.

EBNER, F., CERNY, I., EICHHORN, R., GÖTZINGER, M., PAAR, W.H., PROCHASKA, W. & WEBER, L. (2000): Mineral resources in the eastern Alps and adjoining areas. *Mitt. Österr. Geol. Ges.* **92**, 157-184 (160-162).

EICHHORN, R. (1995): Isotopengeochemishe und geochronologische Untersuchungen an Gesteinen und Mineralien der Scheelit-Lagerstätte Felbertal (Land Salzburg, Österreich). *Münchener Geol., Hefte* **15**.

_____, HÖLL, R., LOTH, G. & KENNEDY, A. (1999): Implication of U–Pb SHRIMP zircon data on the age and evolution of the Felbertal tungsten deposit. (Tauern Window, Austria). *Int. J. Earth Sci.* **88**, 496-512.

_____, LOTH, G., HÖLL, R., FINGER, F., SCHERMAIR, A. & KENNEDY, A. (2000): Multistage Variscan magmatism in the central Tauern Window (Austria) unveiled by U/Pb SHRIMP zircon data. *Contrib. Mineral. Petrol.* **139**, 418-435.

HARRIS, D.C. & CHEN, T.T. (1976): Crystal chemistry and re-examination of nomenclature of sulfosalts in the aikinite–bismuthinite series. *Can. Mineral.* **14**, 194-205.

HODA, S.N. & CHANG, L.L.Y. (1975): Phase relations in the system PbS–Ag_2S–Sb_2S_3 and PbS–Ag_2S–Bi_2S_3. *Am. Mineral.* **60**, 621-633.

HÖLL, R. (1975): Die Scheelitlagerstätte Felbertal und der Vergleich mit anderen Scheelitvorkommen in den Ostalpen. *Abh. Bayr. Akad.Wiss., Math.-Natwiss. Kl.* **157A**.

HORIUCHI, H. & WUENSCH, B.J. (1976): The ordering scheme for metal atoms in the crystal structure of hammarite, $Cu_2Pb_2Bi_4S_9$. *Can. Mineral.* **14**, 536-539.

_____ & _____ (1977): Lindströmite, $Cu_3Pb_3Bi_7S_{15}$: its space group and ordering scheme for metal atoms in the crystal structure. *Can. Mineral.* **15**, 527-535.

KOHATSU, I. & WUENSCH, B.J. (1971): The crystal structure of aikinite $PbCuBiS_3$. *Acta Crystallogr.* **B27**, 1245-1252.

_____ & _____ (1976): The crystal structure of gladite $PbCuBi_5S_9$, a superstructure intermediate in the series Bi_2S_3–$PbCuBiS_3$ (bismuthinite–aikinite). *Acta Crystallogr.* **B32**, 2401-2409.

MAKOVICKY, E. & MAKOVICKY, M. (1978): Representation of compositions in the bismuthinite–aikinite series. *Can. Mineral.* **16**, 405-409.

_____, TOPA, D. & BALIĆ-ŽUNIĆ, T. (2001): The crystal structure of paarite, the newly discovered 56 Å derivative of the bismuthinite–aikinite solid-solution series. *Can. Mineral.* **39**, 1377-1382.

MOZGOVA, N.N., NENASHEVA, S.N., CHISTYAKOVA, N.I., MOGILEVKIN, S.B. & SIVTSOV, A.V. (1990): Compositional fields of minerals in the bismuthinite–aikinite series. *Neues Jahrb. Mineral., Monatsh.*, 35-45.

MUMME, W.G. (1975): The crystal structure of krupkaite, $CuPbBi_3S_6$, from the Juno mine at Tennant Creek, Northern Territory, Australia. *Am. Mineral.* **60**, 300-308.

_____ & WATTS, J.A. (1976): Pekoite, $CuPbBi_{11}S_{18}$, a new member of the bismuthinite–aikinite mineral series: its crystal structure and relationship with naturally- and synthetically-formed members. *Can. Mineral.* **14**, 322-333.

_____, WELIN, E.A. & WUENSCH, B.J. (1976): Crystal chemistry and proposed nomenclature for sulfosalts intermediate in the system bismuthinite–aikinite (Bi_2S_3–$CuPbBiS_3$). *Am. Mineral.* **61**, 15-20.

OHMASA, M. & NOWACKI, W. (1970a): A redetermination of the crystal structure of aikinite [BiS_2 |S| $Cu^{IV}Pb^{VII}$]. *Z. Kristallogr.* **132**, 71-86.

_____ & _____ (1970b): Note on the space group and on the structure of aikinite derivatives. *Neues Jahrb. Mineral., Monatsh.*, 158-162.

PRING, A. (1989): Structural disorder in aikinite and krupkaite. *Am. Mineral.* **74**, 250-255.

_____ (1995): Annealing of synthetic hammarite, $Cu_2Pb_2Bi_4S_9$, and the nature of cation-ordering processes in the bismuthinite–aikinite series. *Am. Mineral.* **80**, 1166-1173.

RAITH, J.G., STEIN, H.J. & HÖLL, R. (2001): Re–Os ages for molybdenites from the Felbertal tungsten deposit, Tauern Window, Austria. *EUG XI Abstr. Vol., J. Conf. Abstr.* **6**, 263.

SPRINGER, G. (1971): The synthetic solid-solution series Bi_2S_3–$BiCuPbS_3$ (bismuthinite–aikinite). *Neues Jahrb. Mineral., Monatsh.*, 19-24.

SUGAKI, A., SHIMA, H. & KITAKAZE, A. (1974): Study on chemical composition of minerals in the system Cu–Bi–S using electron probe microanalyses. 1. Wittichenite (klaprothite). *J. Japan. Assoc. Mineral., Petrol., Econ. Geol.* **69**, 32-34 (in Japanese).

SYNEČEK, V. & HYBLER, J. (1974): The crystal structures of krupkaite, $CuPbBi_3S_6$, and of gladite $CuPbBi_5S_9$, and the classification of the superstructures in the bismuthinite–aikinite group. *Neues Jahrb. Mineral., Monatsh.*, 541-560.

THALHAMMER, O.A.R., STUMPFL, E.F. & JAHODA, R. (1989): The Mittersill scheelite deposit, Austria. *Econ. Geol.* **84**, 1153-1171.

TOPA, D., BALIĆ-ŽUNIĆ, T. & MAKOVICKY, E. (2000): The crystal structure of $Cu_{1.6}Pb_{1.6}Bi_{6.4}S_{12}$, a new 44.8 Å derivative of the bismuthinite–aikinite solid-solution series. *Can. Mineral.* **38**, 611-616.

_____, MAKOVICKY, E., CRIDDLE, A.J., PAAR, W.H. & BALIĆ-ŽUNIĆ, T. (2001): Felbertalite, $Cu_2Pb_6Bi_8S_{19}$, a new mineral from Felbertal, Salzburg Province, Austria. *Eur. J. Mineral.* **13**, 961-972.

ŽÁK, L. (1980): Isomorphism and polymorphism in the bismuthinite–aikinite group. *Neues Jahrb. Mineral., Monatsh.*, 440-444.

Received August 27, 2001, revised manuscript accepted May 18, 2002.